Ultra-flat giant grain Cu film atop α-Al_2O_3 (0001) for apCVD synthesis of graphene

Kevin Roberts

Master's Thesis

Presented to

University of Jyväskylä

2018

Supervised by Johansson Andreas

ABSTRACT

Graphene microelectronic devices are still in the research phase. Consistent production of such small-scale structures requires increasingly higher quality graphene. Commonly, graphene is grown by chemical vapor deposition (CVD) on the surface of a substrate catalyst. Defects on the catalyst are known to generate corresponding defects in the CVD graphene grown atop it. The current study seeks to produce a wafer scale single-crystal Cu thin film supported by Al_2O_3 which is durable enough for apCVD graphene production.

πάντα ρει (*everything flows*) — Heraclitus of Ephesus

TABLE OF CONTENTS

Facts are of not much use, considered as facts. They bewilder by their number and their apparent incoherency. Let them be digested into theory, however, and brought into mutual harmony, and it is another matter. — Oliver Heaviside
'Electro-magnetic Theory II', in *The Electrician* (16 Jan 1891), 26, No. 661, 331.

Overview and Motivation

Graphene may be an integral component of electronic circuits in the future. In their noteworthy prospectus for this new material, Geim and Novoselov review graphene's many unusual properties and the vast amount of research required to exploit them; they speculate that graphene processors are at least two decades away.[1] The long time lag is a consequence of several significant obstacles that must be overcome; one of the first is the lack of a ready supply of high quality graphene. Remember that the definitive graphene studies that elucidated the unusual properties of graphene were accomplished with samples of high quality graphene that were painstakingly acquired. Some were extracted by the low yield exfoliation method (Scotch tape method) that Geim and Novoselov famously used. While other graphene samples, especially today, came from CVD grown sheets.

Chemical vapor deposition (CVD) graphene is on-demand but it comes with the drawbacks that it is expensive, and it is not defect free. Considering first the expense, expect to pay 3 or 4 orders of magnitude more for graphene than gem quality diamonds; pound for pound. Granted, most electronic applications do not need very much, maybe only a few pennies' worth, even at current prices. However, small quantities of graphene pose another problem; they are almost impossible to manipulate. Unless a way to reposition nanometer-scale graphene samples is found, we are stuck laying down much larger sheets and cutting away, and discarding, the graphene that is not needed.

Unlike the expense, the defect problem is less obvious, but much more of an obstacle to research. Graphene's extraordinary properties are known to be detrimentally affected by lattice defects.[2] And all available CVD graphene on the market today is polycrystalline; that is, the graphene sheet is riddled with defects. So, to reliably make large numbers of identical micron-scale electrical devices from graphene, large areas of uniform graphene films must be available.[3] However, as device dimensions decrease into the low nanometer-scale, as is common in modern microprocessor technology, the placement of every single defect in the graphene becomes critical to the device's function. Therefore, the graphene for these applications must be defect-free single crystal.[4]

For one-of-a-kind device research a graphene sheet may be mapped at the atomic level and high-quality regions may be selectively used. Alternatively, devices may be manufactured across a whole sheet of graphene then after post-production testing the substandard devices can be discarded. These methods for getting the best out of defected graphene is time consuming and wasteful and not suited for mass production.

Furthermore, the CVD graphene defects cannot be repaired after the sheet is formed. This is because, such repair of polycrystalline graphene requires the rotational alignment of entire crystals followed by the addition of carbon atoms along the damaged crystal boundaries. These crystal

alignments and defect-free joining of graphene crystals is only energetically feasible at high temperatures in a CVD furnace while the graphene sheet is forming. So, it seems that the way forward requires that, from the start, the graphene CVD process must be improved to eliminate defects.

Chemical vapor deposition (CVD) protocols have been developed for synthesizing graphene on the surface of metal foil[5,6]. Typically, in this process many graphene seeds start growing across the metal surface. Allowed to grow long enough, the individual crystals will merge and form a single sheet of graphene. Typically, the individual graphene crystals are randomly aligned so that their lattices do not match. The resulting crystal boundaries around every nano-crystal of graphene are effectively lines of defects which in turn modify the properties of the sample in an undesirable way. So, one way to improve the CVD process is to either reduce the number of graphene seeds or align the graphene crystals before they merge.

At this time, the most common metal used for CVD graphene is copper. Copper is commercially available and rather inexpensive. Copper foil, as received, is polycrystalline and covered with microscopic milling marks. Used as a substrate for CVD, these Cu defects correlate to graphene defects. Other researchers have reported various methods for improving Cu foil. Commonly, milling marks are reduced by electro-polishing; and crystal size is increased, and overall roughness is improved by high-temperature annealing. These methods do improve the graphene, but the substrate remains polycrystalline which induces defects and lowers the graphene quality.

The current study explores a potentially much improved Cu substrate. The hope is to eliminate both drawbacks associated with Cu foil: polycrystallinity and surface roughness. The goal is to create an atomically smooth single crystal Cu thin film atop polished mono-crystal Al_2O_3. This structure could provide a near-perfect substrate for CVD graphene growth.

THE DESIGN OF THE CURRENT STUDY

The current study explores improvements to the quality of the copper substrate used to grow CVD graphene. It is known that the defects seen in CVD graphene often directly correlate to defects in the underlying substrate. So, an ideal result for this research would be an atomically smooth single crystal copper substrate.

From a variety of substrates that may be used to grow graphene, Cu was selected primarily because Cu is able to form single layer graphene (SLG).[13,14,73,74] Cu supports graphene growth in a surface mediated self-limiting process,[15] and in conjunction with Cu's very low carbon solubility SLG is commonly isolated from this substrate after CVD. As a contrasting example, nickel catalyzes the growth of graphene but its high carbon solubility causes multi-layer graphene (MLG) to precipitate

to the surface when cooled.[16] A secondary reason for choosing Cu; Cu is a rather common and inexpensive metal making it more commercially scalable than other metal substrates.

The production of defect free CVD graphene likely requires that the growth substrate also be defect free. Commonly, CVD graphene is grown on Cu foil, however that substrate is not used in this study because of the disadvantage that foil is always polycrystalline. And, at the initiation of the current study, no known method can remove this faulty characteristic. Therefore, the current study chooses to explore a Cu thin film deposited on a single crystal sapphire (Al_2O_3) wafer chip which has been polished to near atomic smoothness. Cu has been shown to anneal with an epitaxial relation to Al_2O_3 but no such epitaxial relation develops with SiO_2/Si.[17]

A major obstacle to overcome with this Cu/Al_2O_3 stack is to maintain the integrity of the Cu thin film at temperatures near the melting temperature of Cu for sufficient time to grow graphene. Successful production of an optimized Cu substrate would provide a valuable control standard for future optimization studies of other parameters in the CVD graphene process.

Laboratory experimentation is rather time consuming and resource intensive, so it was hoped that computer modeling could be quicker and more cost effective for the task of narrowing the parameter space to be tested.

Computational modeling

One method of constructing a dynamic model uses a bottom-up approach. A first principles (ab initio) model may start with only the atomic number and some structural information as the only input. Predictive models of solids can be made by electronic structure calculations using the density-functional theory (DFT) framework, while using local-density approximation (LDA) or generalized gradient approximation (GGA).[7] In the full-potential, linearized augmented plane wave (FLAPW) method a linear combination of functions, radial wavefunctions and their energy derivatives centered at atomic sites, combined with interstitial plane wave expansion, has been used to predict the high energy structures of heteroepitaxial films of transition metals.[7,8] In calculations related to the current study, FLAPW found the stability of pseudomorphic films, strain distorted crystals at the interface between a Cu thin film and the substrate, is due to the bulk stability of the substrate material, rather than the surface and/or interface effects as usually believed.[7] And ab initio quantum mechanical modeling employing a supercell model, an axial interaction model (AIM), and the projector augmented wave (PAW) method as implemented in the Vienna ab initio simulation package (VASP) have been used to calculate the stacking fault energy and the interfacial energy of the fcc/hcp interface in Cu with 9 atomic layers.[9] Note the limited size and static nature of the these systems.

But additionally, ab initio methods have also been successfully applied to pressure-driven phase changes in materials for about 20 years. Descriptions of these systems depend on energy differences of a few tens of meV/atom and can often be reasonably approximated at absolute zero. However, temperature-driven changes in materials is a different story. Temperature-driven systems rely on energy differences of only a few meV/atom, thus requiring extreme numerical precision. Additionally, as temperature rises new excitations appear and eventually come to drive the transition in question. For the ab initio model to be successful a large phase space must be sampled. Work in this area has just begun; the ab initio models for temperature-driven transitions are only starting to describe the simple elementary metals.[10]

The current study would like to know the dynamics of a Cu thin film from deposition through annealing. But, computer simulation cannot provide the required detail and precision required. In fact, no predictive model has emerged to even map crystal microstructures with their corresponding physical properties.[20] Computational modeling, therefore, was not used as a predictive guide for the current study.

Experimental observation

There are several ways to observe microscopic surface structure and even bulk crystalline structure of samples in a non-destructive way. Thus, by comparing before and after measurements from samples, the dynamics of some transitional phenomena have been documented. But because the data from atomic scale systems is so difficult to record, the underlying mechanisms which drive most observed changes remain undefined. Nevertheless, the experimental literature is found to be far more useful for the current study than the computational literature.

Of all the methods available for examining a sample the quickest and easiest must be the optical microscopy. In the current study, the optical microscope was found, in many cases, to be a sufficient tool for analyzing the samples; because if damage is clearly visible at the resolution of the optical microscope there is no need to use more sophisticated tools to examine it more closely.

Feedback between experimental observation and computational modeling

A correct computational model of the Cu/Al_2O_3 substrate requires that all the relevant parameters of the system be known. Much progress has been made in recent years at mapping near surface crystal orientation using electron backscatter diffraction techniques.[11] Consequently, the associated crystal boundary conditions are better understood. However, experimental verification of the energy profile of the various crystal defects remains unverified by experimental measurements.

As this relates to the current study, the difficulties evaluating thin films at the atomic scale parameters have slowed the feedback experimentalist can give to the model builders who have yet

to find a convergent solution to crystal dynamics. So, at this time, optimization of the Cu/Al_2O_3 system is more likely to be found by systematic experimental trial.

Experimental Results

The desired outcome is an atomically smooth single crystal Cu(111) surface which remains stable for the duration of an apCVD graphene growth cycle; ~40 min. at ~1040 °C. In the current study the Cu is a thin film supported by polished Al_2O_3. After some preliminary experiments, the current study progressed in three stages as described in the following section. 1) Polished Al_2O_3 was tried as a template for single Cu crystal growth; grow that takes place at the time of the room temperature (RT) deposition of the thin film: the outcome was that the Cu was always polycrystalline. 2) Then tried heating the Al_2O_3 to ~240 °C during thin film deposition in a kind of anneal-as-you-go approach: the outcome was that the annealed Cu was always polycrystalline. 3) Then the Miller paper was found. The current setup was not equipped to duplicate the Miller method exactly, so modifications were made to his method to fit the available equipment: the outcome was that one sample was successfully annealed to a continuous Cu thin film without any thermal breakdown.

Preliminary experimental work.

Previous tests in our lab had produced graphene using apCVD techniques on both Cu foil and supported Cu thin film using Ar bubbled through ethanol as the carbon source. Results clearly showed non-pristine graphene distributed across many samples. Defects were discernable using AFM, SEM and the optical microscope included multilayering associated with nucleation sites and disorder associated with grain boundaries and thermal grooves in the copper substrate. Our observations confirm the published research of others and is common knowledge in this field of research: substrate defects translate to defects in the CVD graphene.

Round One: Templated Cu thin film

The first experiments tested a copper thin film supported by polished Al_2O_3, anticipating that the smoothness of the supporting substrate would be transferred to laminar growth of the Cu on its surface.[18] The thin film was deposited by an electron beam evaporator (Balzers) at room temperature, and the unannealed thin film was much smoother than foil as seen in the comparison of the images in Figure 1.Left & Middle. However, during annealing the thin film copper samples were often quickly fractured by thermal grooves as secondary grain growth restructured the copper as seen in Figure 1.Right.

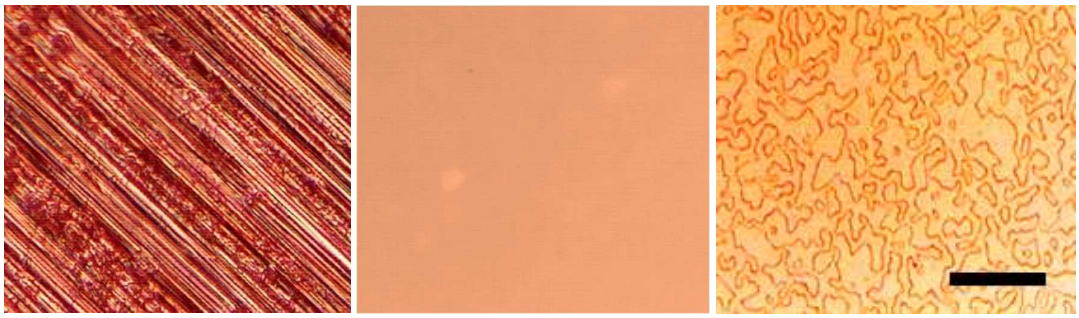

Figure 1 (Left) Unannealed Cu foil. (Middle) Unannealed Cu thin film on supported by polished Al_2O_3. (Right) Annealed Cu thin film with thermal grooves. All samples viewed by a bright field optical microscope at the same scale. (scale bar = 50µm)

To understand better how the thin film developed during deposition the atomic force microscope (AFM) was used to image the surface. AFM images of the Al_2O_3 surface in Figure 2 demonstrate the nearly atomic smoothness of the substrate.

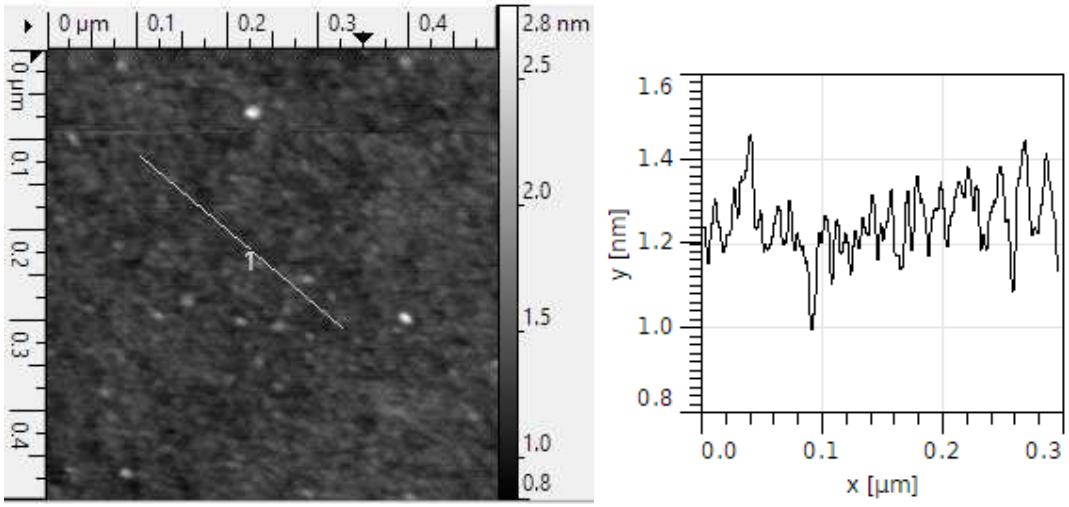

Figure 2 AFM image of the Al_2O_3 surface (left) with exact profile indicating a typical surface variation of about 0.2 nm which is less than the diameter of the atoms.

Figure 3.Left shows a Cu thin film that is about 2 nm thick as calculated from the rate of deposition of 1 nm / sec for 2 secs. Cooberating that thickness value, Figure 3.Right shows the film with an average depth of about the same, assuming the lowest points are at the substrate. However, the Cu surface has clearly taken on a texture that does not follow the smoothness of the underlying Al_2O_3; Cu nanoclusters roughen the surface.

The Cu thin film maintains this nanocluster pattern throughout the thickness of the film as seen on a complete film that is about 0.5 µm thick. In the completed film an additional column-like structure appears, extending up from the surface. As seen in Figure 4 in an AFM image, the Cu nanoclusters themselves clump together to form peaks and valleys. These structures indicate that the Cu has not formed a continuous single crystal.

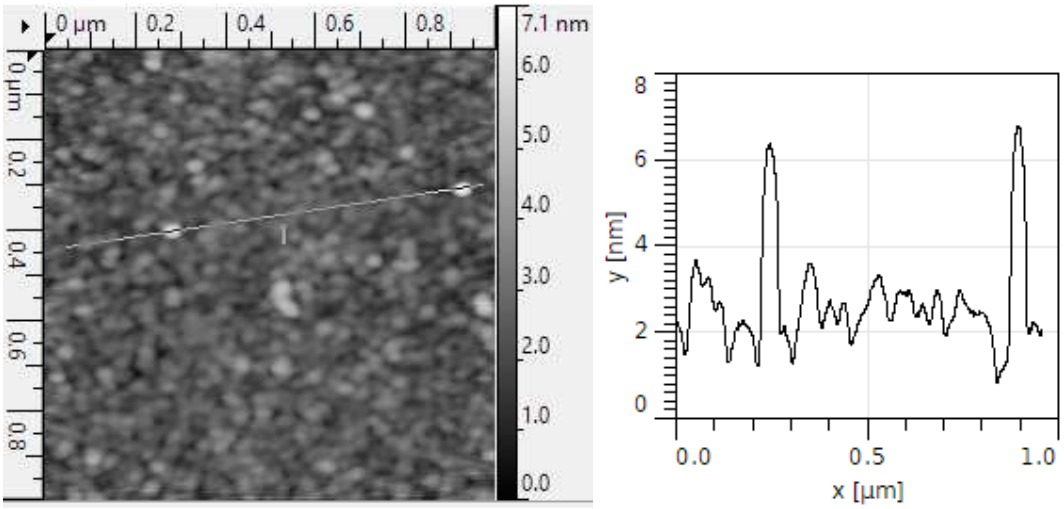

Figure 3 Cu on Al_2O_3. Cu islands form at room temperature when deposited for 2 sec. at 1 nm/sec. Left: AFM image of 1µm X 1µm with exact profile indicated. Right: Profile of the indicated path across the surface.

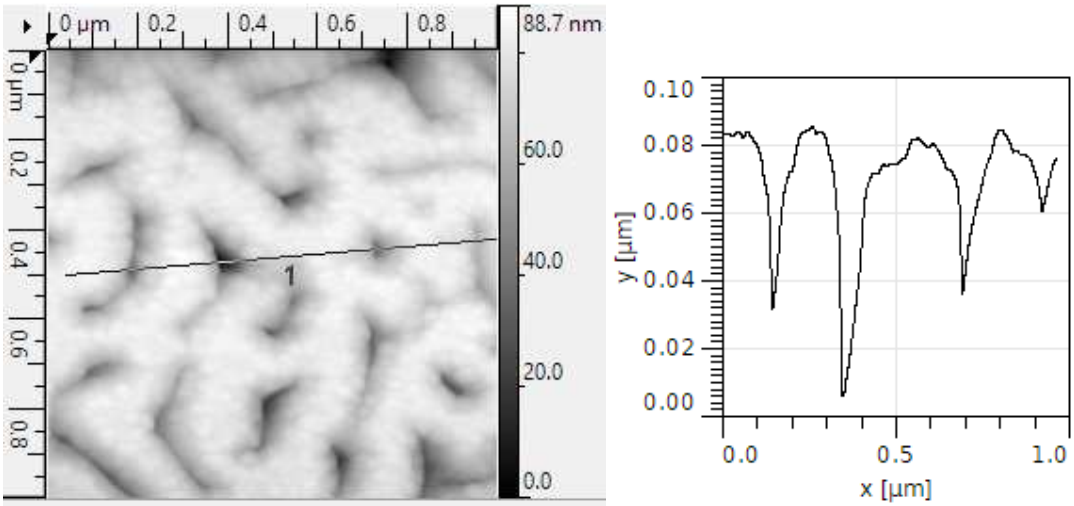

Figure 4 Unannealed Cu on Al_2O_3; thin film deposited at room temperature. Left: AFM image of 1µm X 1µm with exact profile indicated. Right: Profile of the indicated path across the surface. (cu006)

These Cu/Al_2O_3 samples were used in typical apCVD graphene runs. The flow gases were mostly inert Ar, with a low flow of H_2 as a reducing agent, and a low flow of a carbon containing gas, in this case some Ar was bubbled through methanol. A typical temperature for this process was near 1000°C which is sufficient to fully anneal the Cu thin film while remaining below the bulk melting temperature of 1085°C.

Figure 5 shows an AFM image of a single crystal of Cu with atom step edges on a sloped surface. Parallel to the exact profile lines in the image can be seen the close-packed directions of the Cu crystal which extend across the whole image. A close-packed plane is believed to be parallel to the Al_2O_3 surface, while the step edges indicate a change in thickness of the film.

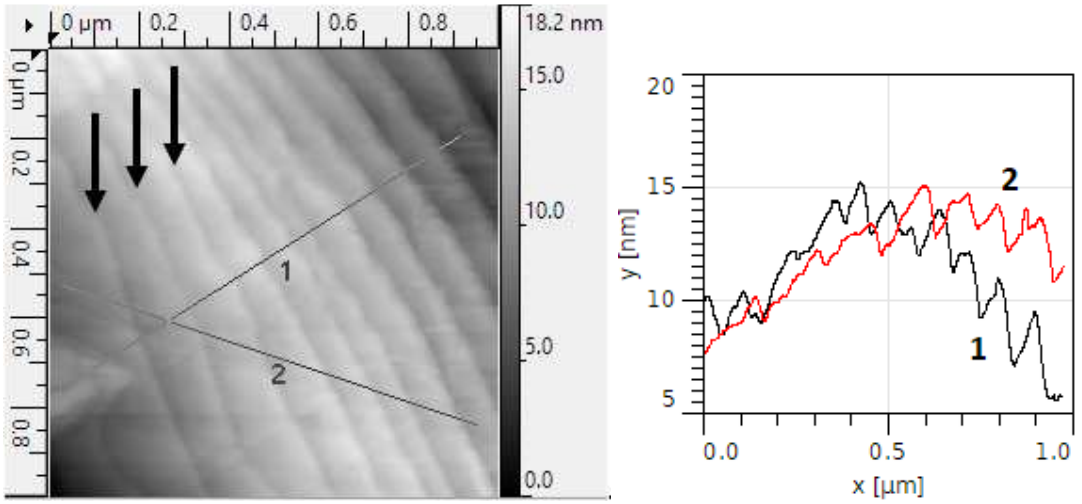

Figure 5 Annealed Cu single crystal on Al_2O_3 with visible step edges (arrows). Left: AFM image of 1µm X 1µm with exact profiles indicated across atomic step edges and parallel to the close-packed directions of the Cu crystal lattice. Right: Profile of the indicated paths across the surface. (cu002)

In a broader view, Figure 6 shows the dramatic thinning of the thin film along a thermal groove. The exact profile across the thermal groove indicates the migratory trend of atoms during recrystallization, in which, atoms are evacuated from the thermal groove and pile up to new heights in adjacent areas.

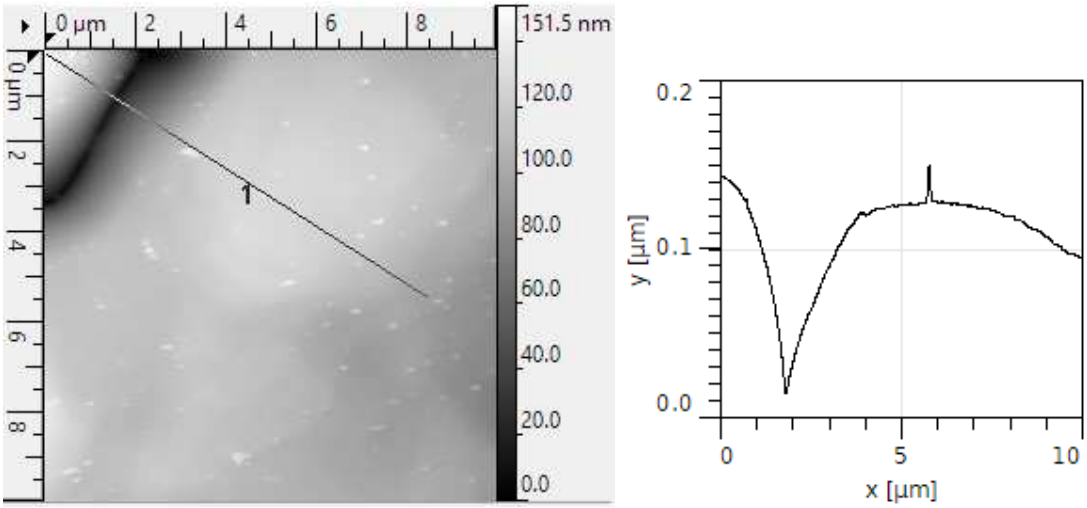

Figure 6 Annealed Cu on Al_2O_3. Left: AFM image of 10µm X 10µm with exact profile line across a thermal groove and debris (light spots). Right: Profile of the indicated path across the surface. Depth of the thermal groove is greater than the thickness of the unannealed thin film, indicating redistribution of Cu during annealing. Debris seen at the 6 µm mark. (cu005)

The conclusion from this round of experiments was that the Cu thin film often suffered extensive damage in the environment of a typical apCVD run.

Round Two: Epitaxial Cu thin film

The second round of experiments tested the claim that heating the Al_2O_3 substrate above 240°C while depositing the copper thin film would result in epitaxial growth of the copper crystals atop the

substrate.[19] This work was a collaboration with Vesa-Matti Hiltunen. These experiments demonstrated the predictions made by Volmert and Weber about epitaxial thin film deposition (more in the theory section below), namely that when the temperature of the substrate is high enough to promote single crystal growth during thin film deposition, out-of-plane islands develop. Then as the islands grow until they meet, misalignment makes polycrystallinity unavoidable.

Whether epitaxial growth was achieved is unknown since the crystalline structure of the sample was not measured directly. However, using AFM, the unannealed thin film was not improved by heating; the upper surface of the resulting copper thin film was rougher. Figure 7 provides an example of an un-annealed Cu thin film which was heated during deposition. The roughness is due to island formation at the early stage of copper deposition, and the added heat energy fuels greater vertical crystal growth.

Annealing of these samples often resulted in more rapid degradation of the copper than in those from the first round of experiments.

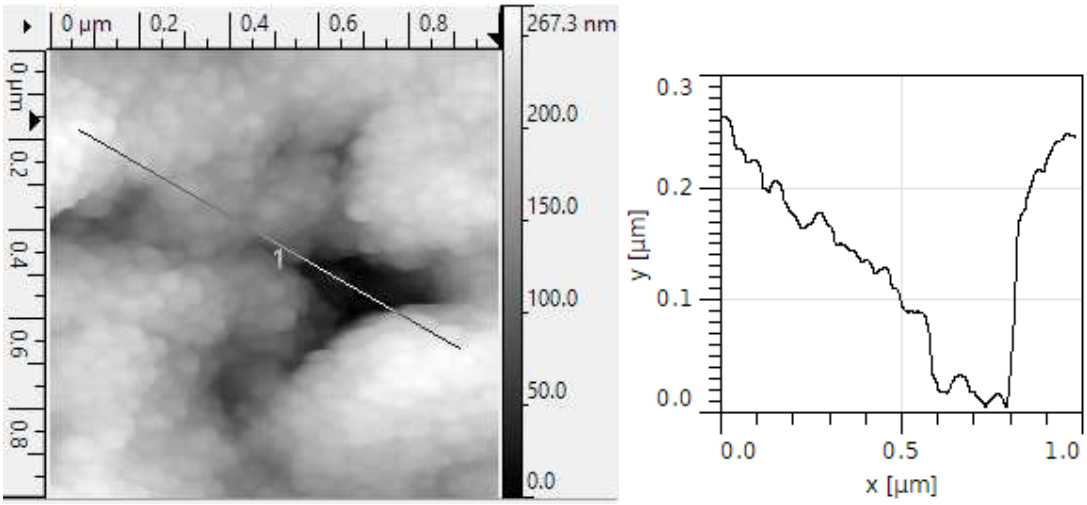

Figure 7 Unannealed Cu on Al_2O_3; thin film deposited at 240°C. Left: AFM image of 1µm X 1µm with exact profile indicated. Right: Profile of the indicated path across the surface. (05271222)

The conclusion from this round of experiments was that heating the substrate during deposition increased the problem of thermal groove formation during annealing.

At this point in the current study it looked like there was no advantage to the Al_2O_3/Cu substrate model over the reported progress made with polished foil. The tested Al_2O_3/Cu always produced polycrystalline Cu, not unlike Cu foil, with the added disadvantages that the Al_2O_3/Cu sample is time consuming to make and degraded rapidly in the CVD furnace. By comparison, the grain boundaries in Cu foil are less destructive to CVD graphene growth than the common thermal grooves that developed in these Cu thin films. However, a negative conclusion to this study was forestalled by an

unusual publication that breathed new life into the thin film model, and a third round of experiments was conducted.

Round Three: Giant grain recrystallization

A third set of experiments attempted to replicate a claim by Miller[43] that a wafer scale single crystal copper thin film could be formed upon annealing, if the deposition of the thin film was carried out with a substrate temperature sustained at 80°C. The key distinction between this and the previous method is that the thin film is deliberately deposited polycrystalline and the single crystal develops by annealing. The indication was that a phase-like change/shift was involved at this deposition temperature which imparted a preferred mixture of crystal orientations distributed within the thin film. This preferred micro-crystal mix seemed to possess an energy profile which was suited to the rapid growth of a copper single crystal when introduced to the elevated temperature of an annealing/CVD furnace.

The experiments in the current study were not designed to replicate the Miller method, rather to adapt or extend the method for the equipment available in our lab. We did not have the equipment to duplicate their work: for example, Miller deposited the copper thin film by sputtering which was unavailable in our lab; and Miller had an annealing furnace with pressure, temperature and gas controls beyond the ranges available from our home-built CVD system. One significant difference with our setup is our furnace is limited to atmospheric pressure, while Miller used lower pressure.

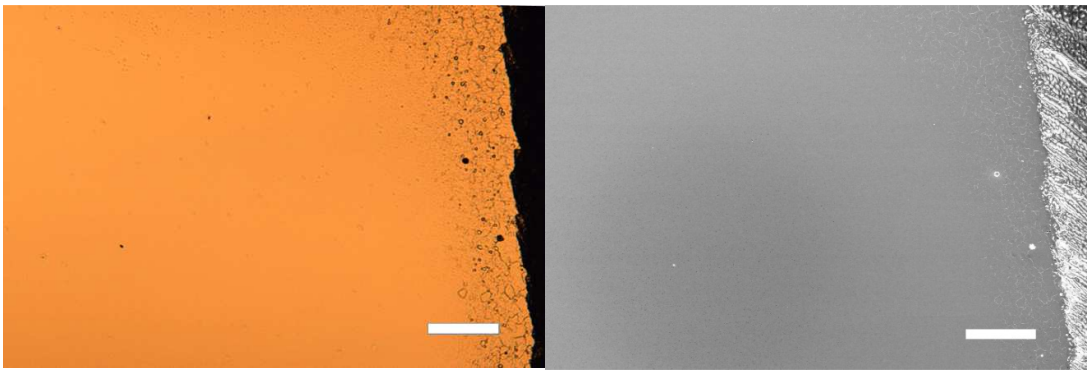

Figure 8 Sample S246-1; 450 nm Cu film on Al_2O_3 after annealing at 1020°C for 40 min. Optical (left) and SEM (right) images of intact thin film. Some thermal grooves or crystal boundaries visible on the area ~100 µm from the edge of the substrate on the right side. Scale bar = 100 µm.

The conclusion from this round of experiments is that a single crystal Cu thin film can be made by the apCVD method. The supported thin film seen in Figure 8 is the solitary sample in this study which exhibited the desired fissure-free Cu surface after annealing. All other thin film samples exhibited the indications of polycrystallinity, including roughness caused by 3D crystal growth and thermal grooves after annealing.

The measured parameters for the successful sample were:

- Al_2O_3 cut on the c-plane and polished on both sides, 5mm square cut from wafer
- New substrate not previously used
- Wet Clean: Acetone, IPA, N_2 blow dry.
- Oxford RIE: O2 Clean
- Thin film deposition in the Balzers: Cu thickness = 450nm, applied to the heated substrate at 82 °C (measure by PT100), deposition rate < 5Å/s
- Annealed by inserting into the already heated hot-wall tube furnace at 1020 °C; annealed for 40 minutes
- Annealing gasses: H_2 at 50 sccm, possibly some Ar flow.

The argon rate is not known with any accuracy. This run was scheduled to be pure hydrogen. It was found at the end of the run when all the gasses were turned off that the Ar flow had been turned on, however the setting is unknown. It is my best guess that the rate was somewhere between 50 sccm and 250 sccm.

So, the current study replicated Miller's results, once! One sample was produced whose features closely matched the goals set forth at the start of this research. This successful sample is an optically near perfect copper thin film substrate that remained absent thermal grooves while being annealed in a CVD furnace with temperature and time profiles suitable for CVD graphene growth. The result has not been replicated despite over 150 samples being processed at or near the same parameters.

Partial replication; the temperature series

Attempts to replicate the single-crystal results have been unsuccessful. In attempts to minimize the effects of processing variation, a series of samples was processed, in rapid succession, varying only the deposition temperature. The results from this series are seen in Figure 9. And while the smoothness of one sample processed at 80°C is smoother and supports the possibility of a single crystal thin film, a companion sample processed using similar parameters fails to duplicate those results.

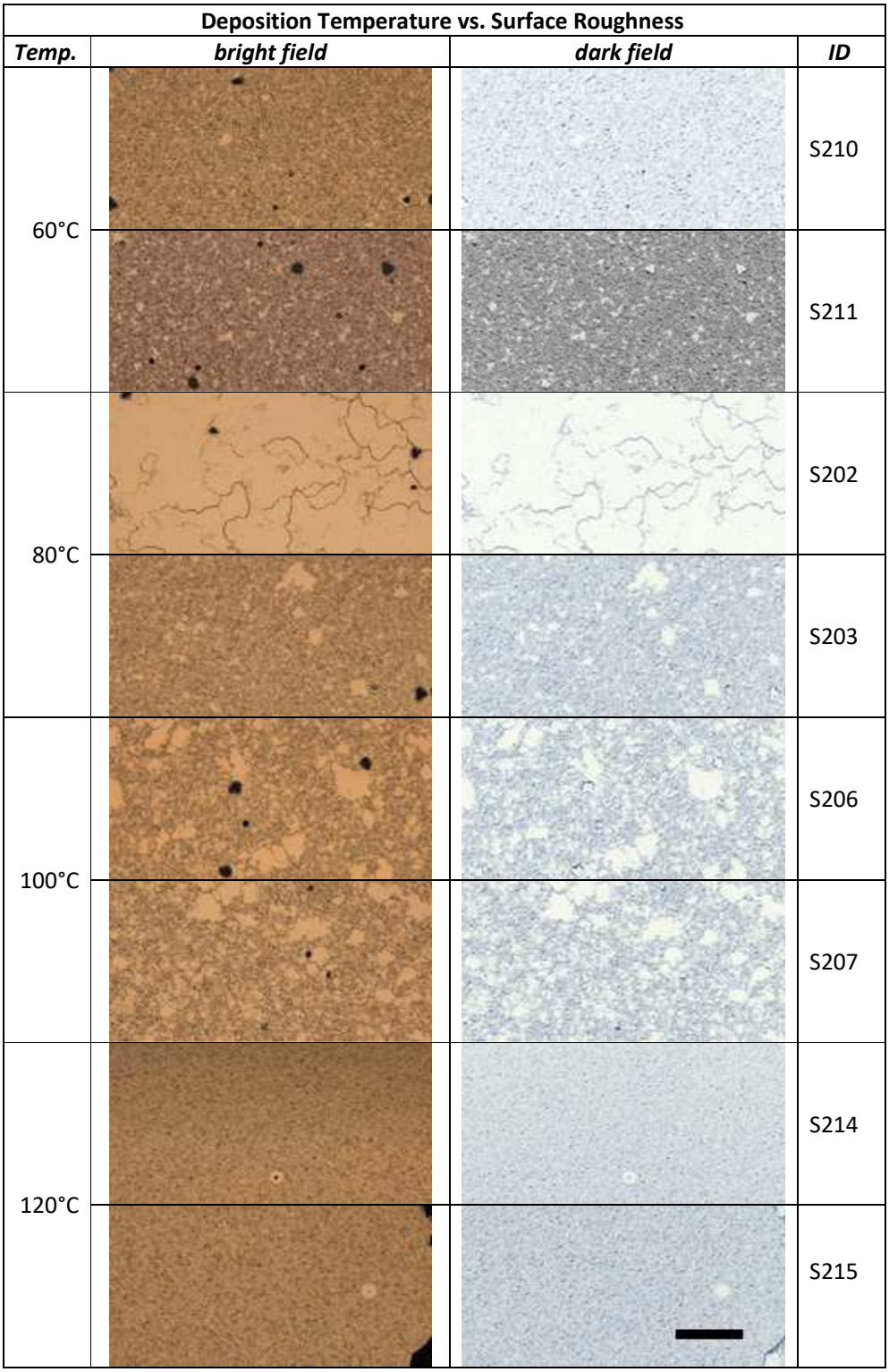

Figure 9 Processing of samples while varying only the deposition temperature. The dark field images have inverted color, so a light-colored area is indicative of a smooth surface. Note sample S202, deposited at 80°C, is much smoother than samples deposited at other temperatures. However, sample S203, with the same processing parameters, does not duplicate the results. All image at the same magnification. Scale bar = 50 µm.

Divergent results

The one sample that recrystallized in the desired way is quite insignificant among all the other samples processed in the current study. Much of the dynamics observed on all these samples is not understood, so some of them are presented here for the interested reader. The current study has been an exploratory research project, and some things observed may be worthy of further examination.

Thermal grooves and texture

The desired surface texture, and goal of the current study, is smooth shiny Cu (Figure 10.A). This texture appeared to be the closed-packed plane as seen in AFM images (Figure 5). But often thermal grooves (Figure 10.B) would form and fracture the surface. But sometimes, seemingly independent of the thermal grooves, rough texture appears (Figure 10.C).

However, sometimes the thermal grooves defined the boundary between the smooth and rough regions as was seen in the early samples that looked like Figure 1.C.

The smooth texture is prominent in the sample in Figure 10.Left, but the rough texture dominates in the sample on the right. In some samples (not pictured) the rough texture covered the entire sample.

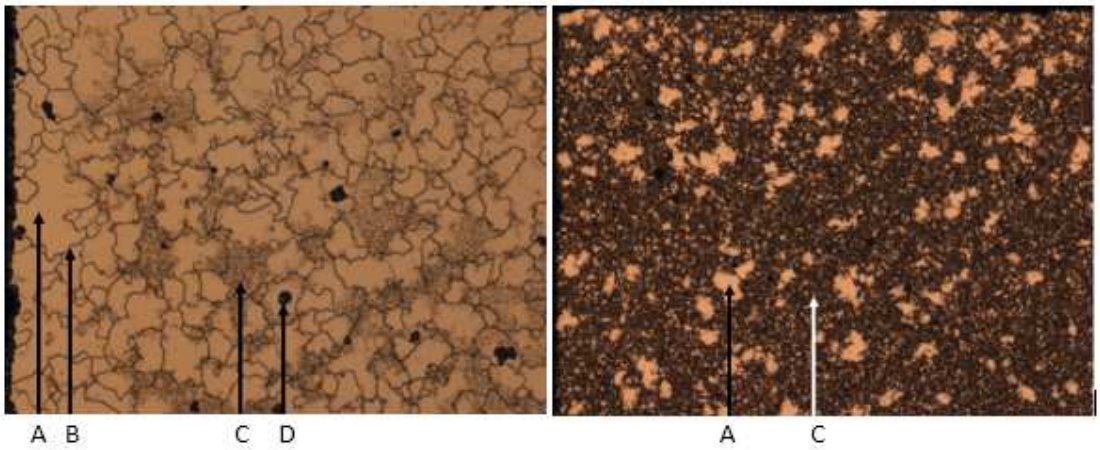

Figure 10 Surface demonstrating competing textures of high and low roughness; with the independently forming thermal grooves and dewetted spots. (A) Low roughness surface. (B) Thermal groove; full thickness fissure through the thin film. (C) High roughness surface; 3D crystal growth. (D) Dewetted spot; often associated with an irregularity on the substrate which may be visible before annealing. (S206-3, S209-2)

Dewetting

Dewetting (Figure 11.B) appears as large patches of exposed Al_2O_3 substrate. The failure of Cu to bond to the substrate may be caused by such factors as: contamination on the substrate (Figure 13.C); chemical preparation of the substrate (which Al_2O_3 plane is exposed, Al or O), hydroxylation of the substrate, thin film deposition temperature, annealing temperature, annealing gases, annealing pressure, and more.

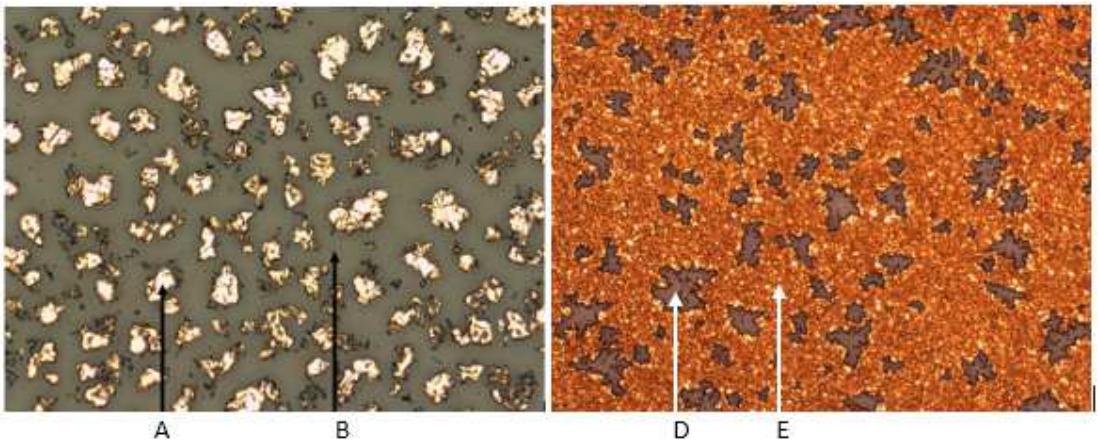

Figure 11 Annealed Cu thin film with dewetting. (A) Island of smooth Cu thin film. (B) Al_2O_3 substrate. (D) Dewetted patch. (E) Rough textured Cu. (mag. x50) (S206-4, S249-1)

Lower temperature annealing and air in the CVD furnace

One set of experiments explored whether annealing at a lower temperature of 400°C was beneficial. The Cu recrystallization was not improved, resulting in a polycrystalline thin film with a rough surface. In Figure 12 the inset of the image on the left is the dark field image of one of these samples; the light color indicates roughness, whereas a flat surface would have been black in this dark field view.

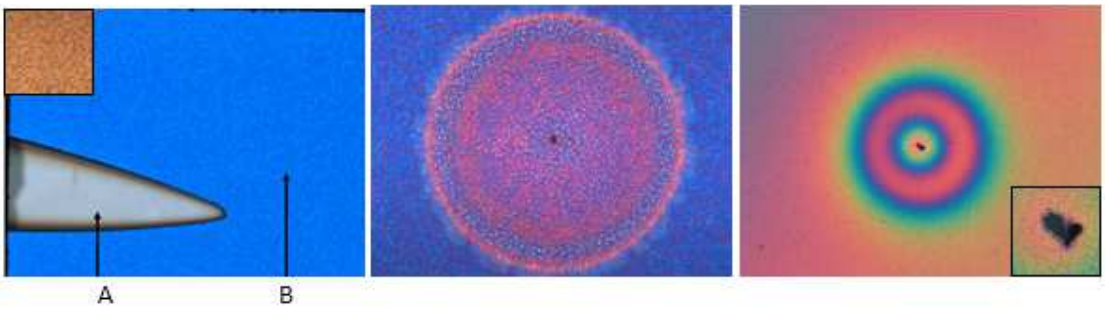

Figure 12 Optical microscope bright field images of Cu thin film annealed at 400°C and exposed to air before reaching RT. All samples are continuous films but have rough texture. The color is like copper(II) nitrate, Cu(NO3)2, and color has a thin film interference component near film defect sites. ***Left:*** *(A) Bare Al_2O_3 from the stage clip shadow. (B) Blue appearance of Cu in bright field view. Dark field image (**inset**) of the sample, illuminated by low angle light, brightness indicates roughness. X50 (S207-3)* ***Middle:*** *Texture and color changes surrounding a central dark object. X500 (S214-2)* ***Right:*** *A patch of Cu has delaminated and hinged up from the surface (**inset**) central to concentric colored pattern. (mag. X50) (S105x)*

At the end of the lower temperature annealing the furnace was flushed with air before the samples had adequately cooled, see the first and second images in Figure 12. Also, in another run N_2 was mixed with Ar and H_2 during the low temperature annealing, see the third image in Figure 12. In these cases, an apparent chemical reaction took place forming possibly copper nitrate or an oxide thin film. The result was a dramatic change in appearance under the optical microscope with the Cu turning a brilliant blue on two samples and an interference spectrum showing in another. Surface

defects, in turn, radiated halos of color and texture changes across the surface, as shown in the image.

A less picturesque but am even more destructive consequence of air in the furnace was seen in the low-pressure tests. The furnace can sustain a low pressure of ~40 mbar with a H_2 flow of 50 sccm. However, the appearance of the samples indicated contamination and total destruction of the thin film. The results of the low-pressure tests ranged from a rough polycrystalline grey colored surface to total dewetting and evaporation of the Cu.

An experiment tested for an advantage to having the samples in the furnace as the temperature was ramped up. With equal volumes of H_2 and Ar flowing the temperature was ramped from RT to 1060°C over 100 min. The samples were then removed from the furnace. The samples were found to be blacken, apparently covered in carbon deposits from the soot on the furnace tube that came into gas phase as the temperature increased.

Balzers: degassing the heated stage

The heated stage was serviced and even rebuild several times. It was found that the stage had to be degassed before using. Degassing involved heating it while in a sustained vacuum. Incomplete degassing resulted in contamination of the sample substrate and failure of the thin film as illustrated in Figure 13. Samples from the Balzers run following replacement of the sample platform and stage-clips were covered with dewetted spots. These spots had straight edges (hexagonal) and at first, were suspected of being small graphene crystals on the Al_2O_3. Raman analysis indicated that no graphene was present on this sample. Rather, the geometry is believed to follow the close-packed directions of both the Cu thin film and the underlying Al_2O_3 crystals. Degassing of the heated stage eliminated the problem as seen in a later sample with similar processing parameters; similar Cu texture without the dewetting, Figure 13.Right.

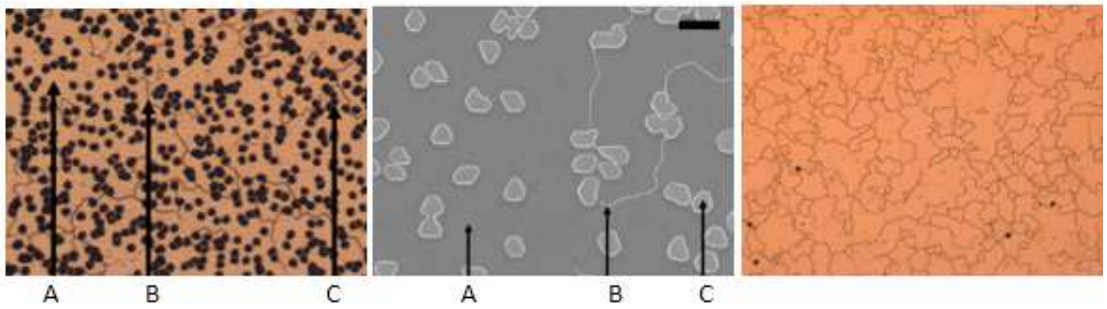

Figure 13 Cu thin films of equal thickness annealed in H_2 flow at 1020°C for 50 min.(left) and 60 min.(right). Left and Middle images of the same sample deposited at 80°C: (A) Smoother Cu. (B) Full-thickness thermal groove. (C) Dewetted spots; straight boundaries associated with the close-packed directions of both the Cu thin film and the underlying Al_2O_3 crystal structure. ***Left****: Optical microscope.* ***Middle****: SEM, scale bar 20 µm. (S213-1) The dewetting was correlated with incomplete degassing after repairs on the heated stage.* ***Right****: Five cycles later, the stage is degassed, and the dewetting spots are almost all gone. Sample deposited at 100°C has similar smooth texture with somewhat higher thermal groove density. (S238-1)*

Stainless-steel stage

At the start of this project the CVD furnace had a sample stage made of Cu. This stage would accumulate carbon during graphene runs, which would burn off after heating in the H_2 flow. But, because of its larger thermal mass it was time consuming to work with, so it was replaced with a smaller stainless-steel stage. The stainless-steel was not stable in CVD conditions. Recrystallization of the stainless-steel on the stage was easily discernable microscopically. And vaporization of the stainless-steel contaminated the samples resting on at as seen in Figure 14.

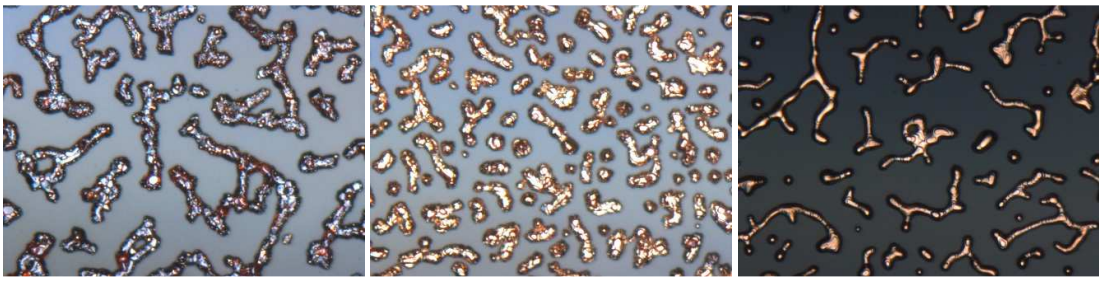

Figure 14 Sample annealed using a stainless-steel stage showing sever dewetting. Left to right, the images are from a single sample showing the progression from the leading edge to the trailing edge with respect to the CVD gas flow. Leading edge Cu is discolored with translucent ruby colored crystals atop the Cu. Transitioning to the trailing edge were most of the Cu is clean, but it has dewetted and evaporated. X500 (S224-1)

Delamination during deposition

The current study used an electron beam evaporator to deposit the Cu thin films. In this setup the Al_2O_3 substrate is mounted in an inverted orientation so that the gas phase Cu leaving the crucible at the bottom of the vacuum chamber travels upwards to be deposited on the underside of the substrate. This configuration is expected to minimize the accumulation of debris on the surface of the sample as such debris should typically fall down to the bottom of the chamber.

However, several samples exhibited micron scale debris on the thin film surface. Most were irregular clumps, while some were flat fakes with irregular borders. Additionally, several samples exhibited defects in the thin film wherein micron scale patches of substrate were visible, that is, the thin film was missing. These patches would typically have irregular borders which had been sharply cut through the full thickness of the Cu film leaving the substrate free of metal. Surprisingly, the surface debris and the missing patches of thin film were found to be directly related.

It was observed in several samples that the irregular debris flakes matched the irregular shape of the patches missing from the thin film. For an example see Figure 15.

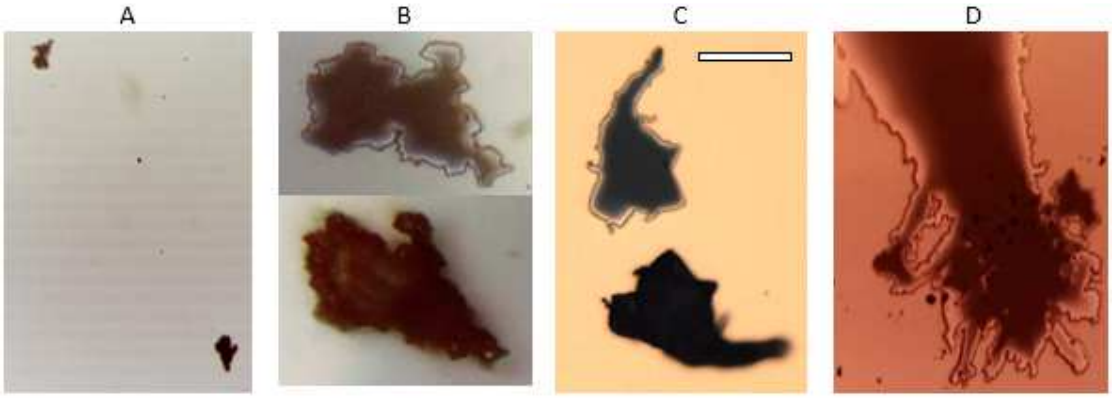

Figure 15 Spontaneous delamination: Newly deposited Cu film (atop polished Al_2O_3), 0.5 µm thick, with delamination hole (A: upper left) and matching delamination lid resting on the surface (A: lower right). The exact scale is unavailable; the objects are estimated to be in the 10's of microns across. Closer view of the delamination hole (B, upper) with sharp irregular boundary, central dark area of Cu free Al_2O_3, and partial thickness Cu thin film near the boundary of the hole indicating that the copper lid first separated from the substrate but remained as a partial shield, then later, jumped to a new location on the underside of the sample. Closer view of the copper lid (B, lower), rotated to more easily compare the shapes. On another sample is seen (C, scale 10 µm) a delamination hole and lid close to each other. Cu delamination near the stage clip site (D) showing light colored Cu film, darker areas of Al_2O_3 substrate and some surface debris. D demonstrates that delamination occurred at various times during the deposition of the Cu film. Spontaneous delamination appears to have an electrostatic component.

Remediation of delamination during deposition

Residual carbon on the Al_2O_3 substrate may cause delamination of the thin film. Likely sources of carbon are from cleaning with hydrocarbon solvents and from previous graphene runs. A reference suggested an Ar plasma etch could remove carbon to undetectable levels.[26,27] Attempts to replicate this plasma cleaning method produced surface damage to the sapphire. The plasma appeared to roughen the surface in spots (Figure 16) across the substrate. Annealing the sample for 2 h in an ultra-high vacuum at 900-1000 °C is reported to recrystallize such surface damage.[27] But since the required annealing chamber was unavailable, this step was not performed.

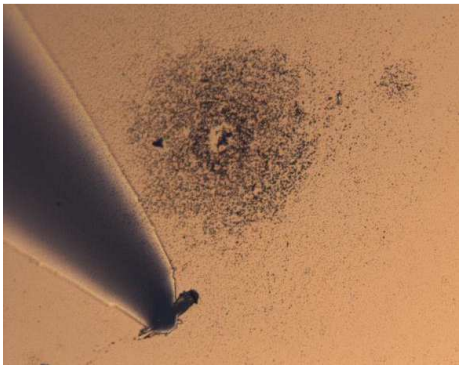

Figure 16 Ar plasma etch damage to the Al_2O_3. The overlaying Cu thin film is also damaged as it overlays the circular pattern etched into the Al_2O_3. The stage clip shadow is seen on the left.

As a substitute for Ar etching, a less aggressive oxygen plasma cleaning process was then tried. This process left the Al_2O_3 surface without any damage observable by the optical microscope, on either the bare substrate or the as-deposited thin film. Furthermore, if the Cu thin film was immediately deposited on the freshly cleaned substrate then spontaneous delamination was not observed.

Exposure of the cleaned (oxygen plasma cleaning) surface to air is known to saturate the surface with water, but this is beneficial because the water reacts with the oxygen rich surface to maximize OH groups on the surface. These OH groups, in turn, will bind covalently to Cu and tightly adhere the first atomic layer of the thin film evenly across the substrate. Note that the tightly bonded Cu nucleates seed crystals which are randomly aligned thus forming a polycrystalline film.

Discussion—surface charge

Some force causes the thin-film to suddenly delaminate and a patch of thin-film is torn away. The observation that the patch may be found adhered to the surface despite the sample being upside-down in the vacuum chamber indicates that there is an electrostatic component to the jumping copper. An electrostatic force presumably draws the dislocated patch back up to the surface. It is observed that this phenomenon happens during deposition, as indicated by some bare patches which were left after copper jumped were then partially covered again by the continuing copper deposition.

Similar in appearance to the isolated patches of jumping copper are the dendritic shaped damage at the border of the shadow from the stage clip, see Figure 15.D. The similar appearance may indicate that the damage was caused by a similar mechanism. Therefore, it is noteworthy that the metal stage clip provides the only electrical path to ground from the newly formed copper thin film. And that if electrical charge where to accumulate on the surface of the insulating substrate, electric current could flow between the grounded instrument and the thin film through the stage clip. Such a current could possibly disrupt the weak bonding between the metallic copper and the substrate, while the effect would be most evident at the location of highest current concentration, specifically near the contact with the stage clip.

Surface charge accumulation

The sample seen in Figure 3 may demonstrate the development of isolated electrical charge on the surface. The sample preparation was an Al_2O_3 substrate which had about 2 nm of copper deposited on the surface in the form of nanoclusters with about 50 nm diameter. As the sample was scanned by AFM, the first pass of the probe returned an unusable noisy signal. However, the second pass of the AFM probe over the same area returned a clear image. By comparison, neither clean Al_2O_3 nor fully formed Cu thin film produced this effect when scanned by AFM. The hypothesis is that electrical surface charge was discharged through the AFM tip on the first pass.

It seems possible that charge could be held isolated on the insulating Al_2O_3 surface until copper islands formed. Charge may originate from the O_2 plasma cleaning. Alternatively, the Balzers electron beam evaporation process ionize some copper which delivers charge to the sample.

It may be possible that the force that removes the spontaneously delaminated patches, arises from electrostatic charge concentration on the surface of the insulating substrate.

Looks like graphene

The tube in the furnace would get covered with soot during other research to grow carbon nanotubes and graphene. No cleaning method had been found to return the tube in the furnace to its original clean state, so a test was run to determine if the carbon was inert and remained bound to the tube walls. A Cu thin film on Al_2O_3 was run through an annealing cycle without an additional carbon source. Figure 17 shows this sample and what appears to be partial coverage of the Cu by graphene domains. However, RAMAN spectroscopy, using a JYU home-built unit, failed to detect anything but copper on this sample.

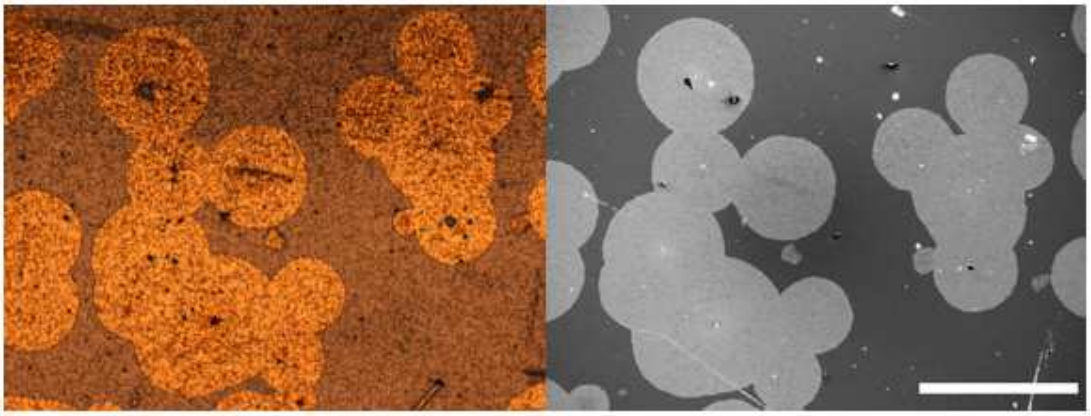

Figure 17 Patterns resembling graphene crystal domains on annealed Cu thin film supported by Al_2O_3 imaged by A) optical microscope and B) SEM. Scale bar 500 µm.

Procedures

The following is a general list of processing procedures.

Al_2O_3 surface preparation

Substrate pretreatment can improve adhesion of the copper film. A high-quality Al_2O_3 surface was prepared as follows:

1) **Wet clean.** Soak in warm acetone and scrub the surface with a cotton swab. Dust and debris is removed and some organics are dissolved. Then rinse in isopropanol and blow dry with N_2.
2) **Ar sputter etch of Al_2O_3 surface.** Using Oxford Instruments Plasmalab:

   program name: Sputter etch Ar

   flow rate: 10 sccm

RF forward power: 100 W

Peak voltage: 600 V

Step time: 60 sec

DC Bias: 367 V

Pressure: 2.50E–05 Torr

The Ar sputter step was expected to remove especially difficult to remove carbon residue.

3) **High temperature anneal.** The Al_2O_3 chips are annealed at 1100 °C for 16 hours in O_2 at atmospheric pressure. This step helps restructure the surface to approach atomically smooth terraces.

4) **O_2 plasma cleaning of Al_2O_3 surface.** Using an Oxford Instruments Plasmalab 80

program name: O_2 clean

temperature: 30 C

forward power: 200W

step time: 120 sec

pressure: 2.5E–05 Torr (Cm gauge 40 mTorr)

The O_2 plasma processing correlates with the cessation of spontaneous delamination of the Cu thin film (jumping Cu).

5) **Hydroxylate the surface.** After the O_2 plasma treatment, the clean Al_2O_3 surface is highly reactive, so exposure to normal atmospheric conditions hydroxylates the surface.

Cu thin film deposition parameters for Balzers Baltec BAE 250 E-beam evaporator

Base pressure: 0.0002 Pa

Deposition rate: < 5 Å / sec

Substrate temperature: heat stage allowed the substrate to be heated from room temperature to over 240°C.

Annealing parameters for the MTI GSL-1100X tube furnace

Base pressure: 1 atmosphere

Available gases: Ar, H_2, O_2, CH_4, N_2

THEORETICAL BACKGROUND

More than a century ago, Bertrand's paradox drew attention to the widely divergent solutions to a seemingly simple statistical problem. It is believed today that the paradox arises from the subtle assumptions made about seemingly insignificant process parameters; the consequence is that many models fail to converge on a single solution.[12]

Bertrand informs this research to find the assumption or process parameter which has been left uncontrolled. What follows is theoretical background and discussion about what may have made the desired single crystal thin film so difficult to replicate.

Copper supported by Al_2O_3

A 5-7µm thick film of Cu was grown on a heated α-Al_2O_3(0001) substrate and found epitaxial when the growth temperature was 240-375°C[19]. And depending on how well this substrate is polished, epitaxial Cu film that is 450 nm thick was grown a temperatures as low as 120°C.[22]

Knowing that copper is a suitable catalyst for graphene and that an epitaxial thin film has few defects, the Cu(111)/α-Al_2O_3(0001) was tested as a substrate for graphene growth. Previous studies show that the Cu(111)/α-Al_2O_3(0001) provide a superior substrate for CVD graphene growth.[33],[17]

The thin film paradox of Volmer-Weber epitaxy

Volmer-Weber[23] describe a type of thin film deposition wherein adatom-adatom binding is tighter then adatom-substrate binding. It is observed that in the Volmer-Weber regime very thin films (< 65 nm), are never fully continuous if deposited at temperatures at or above a critical temperature (T_{VW}). Yet, Volmer-Weber epitaxy requires deposition temperatures at or above T_{VW} to obtain low defect densities within crystalline nuclei. Volmer-Weber epitaxy is illustrated in Figure 18(a).

T_{VW} for Cu deposited on sapphire was found to be dependent on substrate surface preparation, where the most highly polished samples had a T_{VW} < 120°C, while the slightly less smooth sapphire samples had a T_{VW} > 200°C.[22]

Below T_{VW}, a cold adatom, lacking the energy to travel across the substrate, will likely bind at a point near where it lands. So randomly arriving adatoms will form layers with vacancies and dislocations. As the film grows, adatoms cover over the defect sites creating a film that is continuous but that lacks epitaxial character.

Above T_{VW}, adatoms may travel some distance before binding. Migrating to preferred sites, adatoms nucleate islands and grow three dimensionally. Continuous coverage is achieved only when the islands enlarge to the point of meeting. The elevated temperature Volmer-Weber growth mode may produce epitaxial character, but the thin film surface will be rough.

The Volmer-Weber thin film paradox is a choice between small localized vacancies between atoms, or large vacancies between crystals; Volmer-Weber observes that no thin film can be deposited with perfect epitaxy and smoothness.

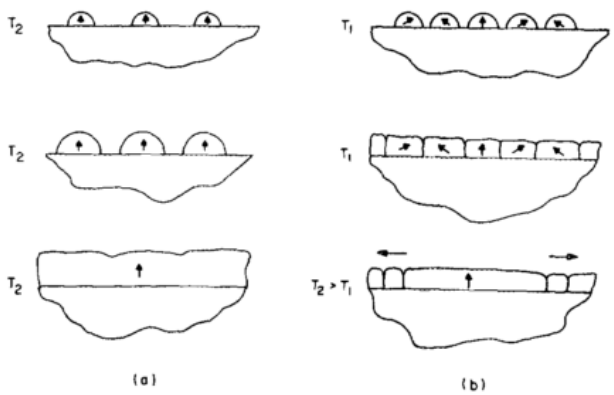

Figure 18 Schematic cross sections of films grown by (a) heated Volmer-Weber epitaxy showing nucleation, island growth and coalescence, and (b) Volmert-Weber epitaxial grain growth showing lower temperature deposition of a polycrystalline film atop a single-crystal substrate followed by epitaxial grain growth at an elevated temperature. (image source[23])

Volmert-Weber epitaxial grain growth

A thin film may not achieve an epitaxial character at the time of deposition. In an alternative path to epitaxy, secondary grain growth may restructure a polycrystalline thin film to impart epitaxial character as illustrated in Figure 18(b). In this mode, metal is deposited at a lower temperature, producing a thinner polycrystalline film. The film inherently has more vacancies and crystal boundaries because of the lower thermal energy during deposition. As deposited the thin film stores tension and compression energy in the crystal defects, grain boundaries, and surface interactions. These energies can be relieved by annealing at a higher temperature.

The lowest energy for the surface of the FCC film tends to be the close packed (111) plane. In the preferred progression, annealing is surface driven, selectively retaining and growing crystals that have a (111) surface while consuming crystals that do not. This dynamic exchange takes place at the crystal boundaries where the barrier potential for atomic movement is greatly reduced, and further reduced by the elevated temperature. At elevated temperatures, the atoms at a crystal boundary are in a state of flux to a depth of several atomic layers. This liquid-like state is driven by the energy difference between the faces of the crystal boundary and is sustained at temperatures well below the bulk melting temperature of the metal.[24] In this surface driven mode, the boundary energy between the substrate and the thin film may be of little consequence thus allowing a substantial mismatch of lattice constants between the two materials. So, while strictly speaking, this mode may not be considered epitaxy, the Volmert-Weber epitaxial grain growth may produce very large crystals, even wafer scale common plain thin film surfaces.

Klokholm-Berry

Klokholm and Berry[25] deposited metal thin films onto substrates at room temperature using an electron beam evaporator, and measured the films' intrinsic stress to be roughly 1% of the

magnitude of the shear modulus for the metals. They propose that the high stresses evolve from an annealed and compacted under-layer constrained by a disordered and less dense surface layer.

When the substrate was heated during thin film deposition, surface atoms could rearrange before being trapped. They found that the intrinsic stress of a metal thin film was small when the ratio of the absolute substrate temperature (T_S) to the absolute metal melting temperature (T_m) was greater than ¼. Calculating the predicted Klokholm-Berry substrate temperature (T_S) for Cu, it is seen to be greater than 67 °C, as follows,

$$\frac{1}{4} < \frac{T_s}{T_m} \cong \frac{340\ \mathrm{K}}{1358\ \mathrm{K}}\ . \qquad \text{Equation 1}$$

Miller's Cu thin film

Miller[43] found that a Cu thin film deposited on α- Al_2O_3(0001) at 80 °C was predisposed to wafer scale grain growth upon annealing. The pre-annealed film is characterized by a nonuniform distribution of grain sizes. And while the surface plane is primarily the close-packed (111) plane, the relationship of the individual Cu grains to the underlying Al_2O_3 is a mixture of OR I and OR II (see Figure 22), where the largest grains are aligned to OR II. The size difference indicates that OR II is favored during deposition.

During annealing however, the OR II grains convert to OR I. The reorientation suggests that there is a small energy difference between OR I and OR II which changes sign between RT and annealing temperature. Miller sees a difference of 3% at RT favoring OR II, and a difference of 4% at 980 °C favoring OR I. This is consistent with the shifting strain between the two materials as Cu expands more rapidly than α- Al_2O_3(0001) with temperature increase.

α-Al_2O_3

Wafers of α-Al_2O_3 cut and polished on the c-plane were chosen for their flatness, chemical and thermal stability, known compatibly with Cu, and their relative low price. More information about Al_2O_3 including crystallography can be found in Appendix I: Crystallography and Appendix II: Al_2O_3.

Surface treatment

A typical sapphire surface cleaning procedure is ultrasonic baths of acetone, methanol and then deionized water. But this treatment leaves multiple atomic layers of carbon containing compounds on the surface. Annealing for 1 h at 1100°C in O_2 reduces the carbon to 0.4 ML (monolayer), while surface carbon remains stable under further annealing.[26]

Carbon is reduced to undetectable levels with Ar^+ sputtering at 1 keV excitation and 25 mA emission for 6 min. [26] However, depending on the environment, Ar ion sputtering can modify the Al_2O_3 surface polymorph, thus roughening the surface. [29] Furthermore, exposure to air unavoidably contaminates the surface with carbon again. [26]

Al_2O_3 / water surface reaction

The fully hydroxylated face of α-Al_2O_3(0001) has an OH group concentration of 15.3 nm^{-2}. The OH groups are neutral making the surface non-polar.[31] The terminal OH group may be coordinated with one, two or three Al^{3+} cations. An ionic structure is most stable when its net charge is nearest zero, and OH termination of the surface approximates this condition better than oxygen.[32]

When temperatures are not too high, hydrogen bonding may take place between neighboring OH groups. At higher temperatures, OH groups loose coordination with metal ions and may be removed from the surface. In this case, the unsaturated metal ions appear as surface Lewis-acid sites.[31]

Air exposure also hydroxylates the surface; partial pressures of water above 1 Torr is all that is required to produce a surface fully terminated in OH. [28] OH surface coverage of 0.44 ML is reported. Water disassociates on the surface to great an ad-OH atop a surface aluminum ion, and an in-surface-OH where the hydrogen interacts with oxygen in the sapphire. (see Figure 19) Cu deposition on this surface proceeds with copper(I) binding associated with the surface OH groups. Surface OH coverage is correlated with improved Cu binding at the α-Al_2O_3 interface. At room temperature, conformal copper(I) coverage reaches a maximum of about 0.35 ML. Copper(I)-copper(I) interactions prevent higher copper(I) density. The remaining thin film is deposited as metallic copper(0). [26]

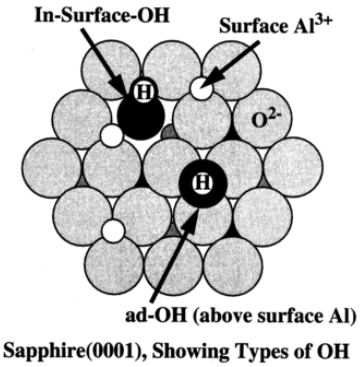

Figure 19 H_2O dissociates on a clean α-Al_2O_3(0001) surface to form one in-surface-OH species and one ad-OH species. An ad-OH prefers to sit atop a surface Al ion. [26]

Copper / Al_2O_3

For basic information about copper see Appendix I: Crystallography and Appendix III: Copper

Appendix III: Copper.

Method for creating a thin film

Metal thin films are often created by some form of physical vapor deposition (PVD). PVD may use thermal, mechanical or electromechanical means to vaporize a metal source in a high vacuum. Because of the low pressure the vaporized metal particles radiate away from the source and travel without collisions until they contact the substrate. Thereby, the application of the metal film is directional, rather than conformal.

The micro-structure of the metal film develops as a function of the energy profiles of the adsorbate and the substrate. Strong adsorbate-substrate interaction leads to laminar (layer-by-layer) growth. While strong adsorbate-adsorbate interaction leads 3D (isolated island) growth. A mixture of these two structures may also be observed in a metal thin film.

Physical vapor deposition (PVD) of a copper thin film onto Al_2O_3

PVD generally describes several methods of sublimating, evaporating or sputtering bulk metal into a vaporized form to be condensed onto a substrate to form a metal thin film. Further descriptions are provided for the method used in this study and additional methods commonly found in the literature used to create similar thin films.

Magnetron sputtering.

Sputtering was used by Miller to deposit the specially prepared thin film. This method uses a beam of inert atoms, such as Ar, which bombards a bulk metal target with enough energy to blast metal atoms off of the surface in a process called sputtering. The sputtered metal atoms fly away in all directions, some of which are deposited as a film on a sample substrate. Figure 18 illustrates the functional components of a magnetron sputtering device.

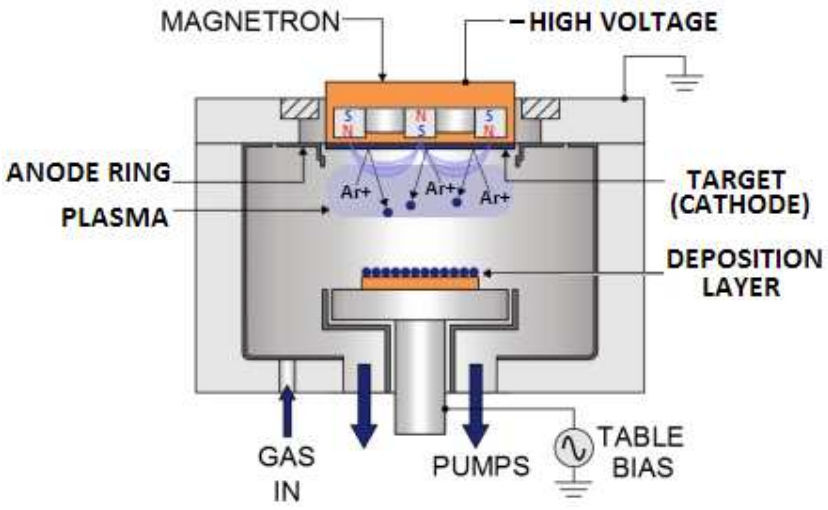

Figure 20 Illustration of magnetron sputtering wherein a target is etched by plasma, and the vapor from the target is deposited on a substrate. (Image: www.oxford-instruments.com)

Electron beam evaporator

Evaporation is the method used in this study to deposit the thin film. Evaporation is achieved by heating a metal ingot, or as in this study, a graphite crucible holding metal, with an electron beam in a vacuum chamber, as illustrated in Figure 21. Vaporized metal atoms fly away in all directions, some of which are deposited on a sample substrate (not pictured).

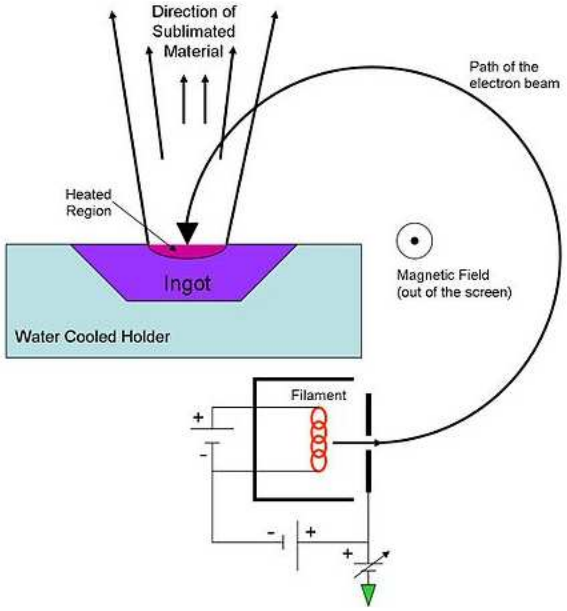

Figure 21 Electron beam deposition circuit schematic. Used in a vacuum chamber, a thin film is deposited onto a substrate mounted in the path of the sublimated material. (Image: commons.wikimedia.org)

Atomic configuration of the copper/sapphire interface

Cu film deposited on Al_2O_3 can form a hetero-epitaxial orientation relation (OR) in which the close-packed planes are parallel to each other. The case where Cu (111) [110]||Al_2O_3 (0001) [10$\underline{1}$0] is commonly called OR I.[27] In another relational case, OR II often refers to Cu(111) [1$\underline{1}$0] ||Al_2O_3(0001) [2$\underline{1}$0]. [30] OR I and OR II are defined this way in the Miller paper and illustration of these ORs is seen in Figure 22. This illustration shows the relative spacing of the two materials when each in a relaxed state. A real Cu/Al_2O_3 interface strains the two materials to accommodate more perfect atomic alignment. The thin film in OR I is expected to be in tension, but OR II is expected to be in compression. The lattice mismatch between Cu(111) and Al_2O_3(0001) is ~+7.0% for OR-1, while misfit strain for OR-II is ~-7.0%.[40,41] Further explanation of these crystal notations is available in the Appendix.

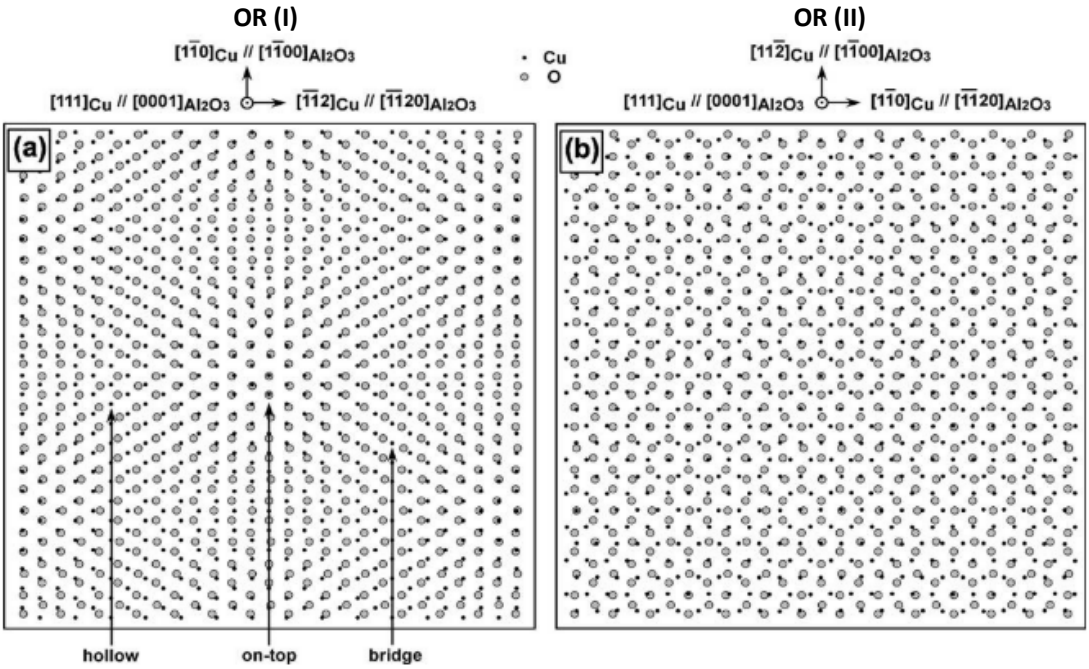

Figure 22 Atomic configurations of the Cu(111)/ Al_2O_3 (0001) interface orientation relationships identified by Miller in pre-annealed samples based on the (a) OR(I) and (b) OR(II), wherein only the atoms of Cu and O closest to the interface are shown. Black dots are Cu atoms, and white circles are O atoms. Note that Cu atoms are illustrated in on-top, bridge and hollow sites of O atoms due to the difference in lattice parameters between Cu and Al_2O_3 crystals.[42]

Residual gas

Bialas and Knoll[22] note that as thin films grow by thermal evaporation they are strongly influenced by 1) contaminants on the substrate, 2) in the source metal and 3) from the residual gas in the deposition chamber. The first, substrate cleaning, is dealt with in another section. The second is minimized by using high purity copper. And the third, gas contamination, is minimized by reducing the ratio of gas flux (J_N) to Cu flux (J_{Cu}) at the substrate surface to a recommended 1/1000.

The gas flux, rate of collisions per unit area and time, to the substrate,

$$J_N = \frac{1}{4} n \bar{v}_{th} = \frac{1}{4} \cdot \frac{p}{kT} \cdot \sqrt{\left(\frac{8kT}{\pi m}\right)} = \frac{p}{\sqrt{(2\pi m k T)}} \qquad \text{Equation 2}$$

where n : number density, $\bar{v}_{th}$: mean thermal velocity, p : chamber pressure, T : absolute temperature, and m : particle mass. At room temperature $T = 293$ K, in a chamber purged with nitrogen gas,

$$J_N = \frac{p}{\sqrt{(2\pi(4.65173 \times 10^{-26})(1.38065 \times 10^{-23})(293))}} = 2.91 \times 10^{22} \cdot p \ \ \mathrm{m^{-2} \cdot s^{-1}}$$

The Cu flux to the substrate,

$$J_{Cu} = \frac{\rho_{Cu}}{m} \cdot r \qquad \text{Equation 3}$$

where ρ_{Cu} : density of Cu, and r : deposition rate in terms of thickness per unit time.

$$J_{Cu} = \frac{8920}{1.05521 \times 10^{-25}} \cdot r = 8.45 \times 10^{28} \cdot r \ \ \mathrm{m^{-2} \cdot s^{-1}}$$

For a typical chamber pressure and deposition rate used in this study,

$p = 1.2 \times 10^{-5}$ mbar (1.2×10^{-3} Pa), and $r = 4\ \text{Å} \cdot \mathrm{s^{-1}}$.

$$\frac{J_N}{J_{Cu}} = \frac{(2.91 \times 10^{22})(1.2 \times 10^{-3})}{(8.45 \times 10^{28})(4 \times 10^{-10})} = 1.03$$

So, the gas flux to Cu flux ratio for this study is calculated as being three orders of magnitude higher than the literature recommends, so, not ideal. However, heating the substrate while cooling the chamber walls may help reject gas from the substrate while trapping gas on the walls.

Interface chemistry

Hydroxylation of the α- Al_2O_3(0001) surface greatly promotes binding of Cu to the substrate thus suppressing the growth of 3-dimensional metal islands. As Cu is deposited the hydroxyl groups stabilize Cu(I) across the surface, thus wetting the substrate with Cu, with the resulting 2-dimensional surface coverage. The surface reaction is[26],

$$\mathrm{OH^- + Cu^0 \rightarrow\ O^{2-} + H + Cu^{1+}} \qquad \text{Equation 4}$$

The Cu(I) strongly adheres to the Al_2O_3 surface[34],[35]. And while Cu(I) amounts to only ~1/3 of the initial monolayer it adequately anchors the copper and initiates continuous coverage. Additional copper deposition forms 2D metallic Cu(0) layers creating a laminar metal film. The Cu(I) in the presence of Cu(0) is thermally stable up to 430°C. The consequence of elevated temperatures is the dehydroxylation of the surface, followed by the nucleation of 3D metallic crystals. Sustained elevated temperature leads to secondary crystal growth which can result in dewetting of the Cu(I) from the Al_2O_3 substrate. [34,36,37]

Eutectic bonding may be used to laminate a copper wafer or foil to a sapphire substrate.[38] The process begins by oxidizing the copper surface. The cupric oxide (CuO) will provide an oxygen source for the eutectic reaction. Then the copper and sapphire are laid together and heated in a tube furnace in an Argon atmosphere. At a temperature slightly below the melting point of copper (1065°C < T < 1085°C) a liquid eutectic mixture forms between the copper and sapphire. As the interface is wetted by this liquid the copper and sapphire layers are drawn together. Subsequent cooling and solidification of the eutectic layer produces a continuous bond between the two substrates.

The eutectic mixture is Cu/Cu_2O which chemically bonds to the Al_2O_3. A small amount of aluminate ($CuAlO_2$) also forms in this process and it can tightly bind to either the Cu or Al_2O_3.[39]

Un-annealed treatment of copper film

Miller[43] deposited Cu film on a whole wafer which was then coated with PMMA. The protected wafer was then diced. After dicing, the PMMA was removed with acetone, then isopropanol. This

processing step was not tested in the current study. This may be important if residual carbon remains on the Cu since it could form graphene in the annealing furnace; and graphene has been reported to protect the underlying Cu catalyst from excessive evaporation at CVD temperatures.[52,53]

Cu on MgO

Using MgO(111) as the support for Cu(111) the thin film produces no apparent in-plane rotational disorder of the Cu, therefore no twinning.[44] Therefore, MgO may be superior to Al_2O_3 as a support material.

Atmospheric pressure chemical vapor deposition (apCVD)

This section is about the apCVD graphene process only as it relates to the Cu/Al_2O_3 substrate.

Furnace

The furnace used is MTI GSL-1100X-220V-50, with a 2" quartz tube. This tube is too small to accommodate a full wafer.

CVD temperature

The quality of graphene grown by CVD on Cu generally improves with increasing temperature. But, the upper limit for the temperature of this system is, therefore, just less than the melting temperature of Cu.

The first rounds of experiments in the current study tried to find if as-deposited thin film could be manufactured with a microstructure that is stable, without significant change, at CVD temperatures. The final rounds of experiments in this study tried to find a thin film that could anneal to be stable.

CVD pressure

Many studies are using low pressure in the CVD furnace. Our attempts to replicate these conditions were not successful at anneal Cu or growing graphene. Extreme dewetting of the Cu thin film and discoloration of copper substrate indicated that air was leaking into the chamber. So, we opted for atmospheric pressure CVD (APCVD).

To maintain the required low partial pressures of the active gasses, back pressure was supplied by the inert gas, Argon. The gases were metered individually by mass flow controllers and delivered to the chamber at atmospheric pressure.

CVD gases

The metered gases available and useful to the current study include Ar, H_2, and CH_4. Additionally, trace amounts of oxygen is expected 1) as a contaminant in the metered gases, 2) from the atmosphere during transfer to the furnace, and 3) released from the surfaces of the furnace, loading rod, and substrate especially when heated. Atmospheric N_2 may also enter the furnace

during loading. The continuous flow of metered gas is expected to rapidly flush away atmospheric gases when operating the furnace.

As gas enters the heated zone of the furnace gas phase reactions can occur. One disadvantage to the apCVD setup is that longer chain carbons are more stable in the gas phase[48] and pose an additional source for contamination. To minimize the deposition of soot on the samples the furnace was redesigned to make sample loading in the upwind direction instead of the sooty downwind/exhaust direction. Graphene quality improved with this modification.

Argon

Argon functions as an inert transport gas while providing a large portion of the partial pressure.

Hydrogen

Primarily, hydrogen functions as a reducing agent, binding oxygen. Hydrogen may also participate in other CVD reactions during graphene growth. Hydrogen is also soluble in Cu and may play a physical role in the annealing process.

Carbon

The carbon, in the form of hydrocarbons, fed into the CVD furnace was ethanol, in the first studies, and methane in later studies. Ethanol was vaporized by bubbling hydrogen and/or argon through refrigerated ethanol. This method provides poor hydrocarbon rate control and was eventually abandoned. Methane is more easily controlled since it can be metered by a mass flow controller (MFC). Both hydrocarbon feedstocks undergo gas phase reactions and form higher mass compounds, and the stability of larger molecules increases with the pressure in the chamber.[48] Consequently, soot can build up at the exhaust end of the furnace, and the same chemicals can be deposited onto the sample substrate causing high density nucleation and multilayer formation.[49]

Oxygen

Even ultrahigh purity (UHP) hydrogen contains oxygen impurities.[47] Our setup does not include any additional oxygen removal system; so traces of oxygen are always present. Oxygen is expected to participate in some gas phase reactions, for example in the formation of water vapor and carbon monoxide. While on the substrate surface, oxygen and oxygen containing compounds play a dual role; 1) reducing graphene growth by passivating some active sites thus limiting nucleation and multilayer islands[50], and by etching carbon from graphene edges, and 2) increasing graphene growth in the reported case of water vapor stimulating the formation of multilayer graphene[51]

Graphene on Copper

Graphene capped copper is reported to increase copper surface grain size by reducing overall Cu sublimation[52]. Also, graphene atop copper decreases the rate of thermal groove formation[53]. In the study of ref. 53, LPCVD graphene was grown at 1030C in hydrogen and methane on top of copper foil which had been annealed in hydrogen. X-ray photoelectron spectroscopy (XPS) established that

the copper's concentration of nitrogen and oxygen impurities were unchanged after annealing and graphene growth. This is significant because surface oxygen on copper has been reported to reduce the number of nucleation sites for graphene.[54] So, the implication is that exposing the pre-annealed copper to oxygen may be sufficient to repress the proliferation of graphene seed sites.

In the key reference paper for giant copper grain growth[43], the copper thin film was processed before annealing for the purpose of protecting the thin film during wafer dicing. The newly deposited copper was spin coated with PMMA, which was later removed by washing with acetone and then isopropanol. This processing undoubtedly deposited a liberal coating of oxygen and carbon rich ad-atoms to the copper surface. At annealing time, great care was taken to remove oxygen from the LPCVD gases to a level of ~1 ppb. The total pressure of 5.3 kPa (50 Torr; 53 mbar) is characterized by the authors as providing back pressure to suppress sublimation.

Annealing

Thermal energy transferred into the thin film allows for annealing. In the current study, like in the Miller method, a hot wall tube furnace is used. This setup eliminates the possibility that heat is transferred up through the substrate to the substrate/copper interface and on up through the thin film; as would be the case in of a heated-stage-type furnace. To reiterate, the thin film is being heated and annealed starting from the exterior surface. This energy flow is noteworthy for the later evaluation of the annealing dynamics of the Miller process.

Annealing dynamics

The copper is annealed to increase the crystal size and to smooth the surface. The thin films are annealed in the CVD furnace at temperatures from 950 to 1060 °C. Ideally, secondary crystal growth restructures the thin film to form a monocrystalline surface. However, since copper is conserved in the process, the growth of one crystal necessarily requires that other crystals be consumed. This dynamic restructuring may lead to decreased thickness along crystal boundaries. Known as thermal grooves, these defects can lead to complete dewetting of the substrate along the crystal boundaries.

Copper can also evaporate in the furnace, so given enough time and heat, thermal grooves will always appear in the copper thin film. But several factors can help prevent rapid onset:

- Clean the substrate to enhance copper's adhesion to the substrate.
- Back pressure from inert gas.
- Increased copper partial pressure (Cu foil pocket, upstream Cu source, clean Al_2O_3 laid on top of the Cu thin film)
- Remove oxygen from the Cu. Oxygen contained within the copper film (even from native oxides) forms water when hydrogen is a constituent of the annealing gas. As the copper anneals the resulting water vapor bubbles generate micro-voids in the copper

crystal structure. Large deformations of the film occur because of the internal pressure.[45]

Grain Growth (Normal Grain Growth)

As deposited, the thin film retains energy in the form of stacking defects and grain boundaries. At temperatures starting at well below the bulk melting point (T_m) atom movement is driven by this stored energy. Grain boundaries are seen to move as atoms migrate to locations that reduce the total energy stored in the film. Normal grain growth is observed when all grain boundaries move at about the same rate. As this mode progresses total grain boundary length decreases as some grains are consumed. The texture of the film coarsens as the average grain size increases. Normal grain growth demonstrates mono-modal change in grain size; all growing grains grow at the same general rate.

Secondary Grain Growth (Abnormal Grain Growth)

Secondary grain growth is observed when grain growth is bi-modal; when some growing grains increase in size at a significantly greater rate. This unusual, or abnormal, growth mode may result in a single grain consuming all other grains.

Opposition to Grain Growth

Evaporation and sublimation allows gas phase Cu to leave the thin film permanently, which naturally does not contribute to grain growth.

Thermal grooves are lines of significant thinning along grain boundaries caused by heat. Heat mobilizes the migration of atoms in the grain boundaries during annealing because atoms in the boundary are less tightly bound to the solid than the atoms in the bulk. Any surface mobility that may occur will tend to remove atoms from boundary. Given enough annealing time, grain boundaries will lose material causing the film in the grain boundary to thin and eventually to dewet from the substrate. Thermal grooves are the prelude to the formation of isolated islands and total destruction of the thin film.

Impurities, such as carbon, migrate to the grain boundaries where they obstruct the diffusion of the pure metal from one grain to another. Grain growth stagnates as a result. Additionally, hydrogen and sulfur can remain bonded to copper at temperatures in excess of 400°C, while the effects of these impurities remains unknown.[46]

Seed crystals

Miller[55] once deposited a thin film using a TEM grid as a shadow mask and observed that when annealed giant grain growth did not occur in most of the thin film squares. Miller concluded that a seed crystal must be required and that the density of seeds was only about 1 per mm^2.

Surface to substrate annealing

In surface-to-substrate annealing, heat mobilizes the atoms with the most free energy, namely surface and crystal boundary atoms. Surface driven recrystallization occurs when atoms arrange in the low free energy close-packed (111) plane; typically, nucleation occurs at multiple sites producing a polycrystalline surface. These surface crystals then grow downward as annealing progresses. Annealing can continue to penetrate into the metal as crystal boundary atoms become mobile and recrystallize onto the seed crystals.

This mode of annealing does not correspond to the Miller annealing mode because this mode creates random OR alignment while Miller produces OR I exclusively.

Substrate to surface annealing

Annealing starts with the atoms that possess the highest free energy. So, initiating annealing at the substrate's surface is more likely when the sample is annealed on heated stage. As the heat energy moves up through the sample recrystallization may start with epitaxial seed formation with the close-packed plane parallel to the substrate. While these seeds may be aligned with each other, twinning may be commonplace because of lattice mismatch.

Like the Miller mode of annealing this mode can produce metal crystals which are aligned with the substrate. However, this mode of annealing does not correspond to the Miller annealing mode because Miller uses a hot wall annealing furnace.

Lateral surface annealing

Xu in a recent paper[56] describes a lateral zone melting technique used on foil to form a single Cu crystal on the surface. Foil has much larger crystals than the optimal pre-annealed Miller thin film. The lack of free energy stored in boundary defects (as in a Miller sample) was overcome by Xu by migrating a narrow beam heat source laterally across the surface with sufficient heat to melt the surface atoms. As the beam passed the melt could then cool and recrystallize. An appropriate seed crystal may form which stretched across the full width of the sample. In this case, the whole surface becomes a single crystal as the sweeping melt zone recrystallizes onto the seed.

Xu mode annealing does not correspond to Miller mode annealing because the surface driven seed formation would not predictable align with the substrate crystal.

Lateral interface annealing

The speculation is that the Miller mode of annealing must progress laterally along the interface between the Al_2O_3 and Cu. This mode is required to achieve the OR I alignment. Annealing may be initiated at the interface, even in a hot wall furnace, because the difference in thermal expansion between the materials generates strain energy at the interface. Continuing this line of reasoning, Miller's seed crystal is likely spontaneously formed at the cut edge of the sample, at the interface,

since these interface atoms have the highest available free energy. It seems possible that interface strain energy is released very rapidly with a wave of lattice hopping sweeping across the sample at the interface. From the interface a wave of shifting atoms could lift up to the surface, driven by heat and the energy stored in lattice defects.

Terminology

Recrystallization: Also called secondary crystallization or abnormal crystal growth, recrystallization is the movement of atoms from one crystal site to another. This process is characterized by a coarsening of the crystal structure wherein some crystals are consumed to grow other crystals. Total crystal boundary area within the thin film is diminished during this process as some crystals are completely consumed. Recrystallization is driven by localized site energy differences, where an atom moves from a higher energy site to a nearby lower energy site activated by absorbing the energy required to overcome the barrier potential. Recrystallization exchange sites may occur at the thin film surface, between crystal boundaries, at internal crystal defects, or along the thin film/substrate boundary. Some recrystallization can occur in a thin film at ambient temperature[58], however chilling to below –20°C is observed to suspend this process[61].

Recrystallization is a process that minimizes the available free energy, and it may provide short term improvements to the quality of the thin film. However, since a flat thin film is never the lowest energy structure for the metal/substrate pair, eventually recrystallization will destroy the thin film. Recrystallization will eventually result in 3D crystal growth which causes thickening in places, at the expense of the film thinning along the crystal boundaries. Destruction of the thin film occurs as thermal grooves partition the film along crystal boundaries.

Annealing: Energy can be added to a crystal to accelerate recrystallization or to advance the degree of recrystallization to remove higher energy defects. For example, annealing is a process of heating a crystal and then slowly cooling it. The annealing thermal cycle provides the activation energy to minimize stored energy within the crystal. Annealing advances recrystallization by increasing the average crystal size and decreasing the crystal defect density.[62,63,64] Defect removal includes rearranging the atoms of the pure metal to eliminate stacking faults. Annealing can also migrate impurities from the bulk of a crystal out to the crystal boundary.[46]

Typical annealing is characterized by the bulk temperature being raised to somewhere below the bulk melting temperature. Also, a material undergoing typical annealing has an initial state with high crystal volume to boundary volume ratio; that is, larger crystals packed closer together. Despite the temperature being sufficient for crystal boundary migration, the polycrystallinity remains after annealing. This is because there is insufficient energy to rotate individual crystals to form giant

crystals, likewise, there is insufficient energy to melt the existing crystals to allow giant grain recrystallization.

The **Czochralski process** is characterized by starting with a single seed crystal which is dipped into melted material at a temperature critically close to the melting temperature. Giant crystal growth proceeds as recrystallization occurs at the faces of the seed.

The **Xu process** is claimed by them to be like the Czochralski process.[56], but I believe qualifiers are order. In contrast to Czochralski, Xu does not start with a preformed seed crystal, but rather, allows the seed to form spontaneously as the melt zone weeps past the edge of the sample. Surface driven forces form and orient the seed to form a 111-plane, and the receding melt zone recrystallizes seamlessly at the surface (shall we call it 2D Czochralski). Once again, unlike Czochralski, the Xu's whole sample is not single crystal, only the surface is, underlying material never melted and remains polycrystalline. By comparison to the Miller process, the Xu process seems to provide much more control of the energy required for recrystallization.

The **Miller process** starts with a specially prepared pre-annealed thin film which is polycrystalline. After some unknown dynamics at sub-melting temperatures, the annealed thin film is a full thickness single crystal with (111) plane surface, with the Cu crystal specially aligned with the Al_2O_3.

Table 1 provides a summary of the characteristics of these various annealing modes.

Table 1: ***SUMMARY OF ANNEALING MODES RELEVANT TO THE CURRENT STUDY***

Process	**Initial XTL structure**	**Max. Temp.**	**Significant XTL-growth mode**	**Final XTL structure**
Typical Annealing	Large XTLs	$< T_m$	High energy XTL faces are consumed to recrystallize on lower energy faces. XTL boundaries migrate	Fewer XTLs, larger average XTL size
Miller	Some large OR II, much small mixed OR.	$< T_m$	OR II anneal to OR I. Mechanism unknown.	Mono-XTL surface.
Czochrolski	Single XTL	Seed $< T_m$ in contact with liquid	Recrystallization	Mono-XTL bulk
Xu	Polycrystal foil	Surface sweep zone $> T_m$	Spontaneous formation of a single surface seed, then recrystallization to that surface XTL.	Mono-XTL surface.
Zone melt	Polycrystal bulk solid	Bulk sweep zone $> T_m$	Spontaneous formation of multiple seeds, then bulk recrystallization	Poly-XTL bulk
Typical Melting	Liquid, non-XTL	$> T_m$	Spontaneous formation of multiple seeds, then recrystallization	Poly-XTL bulk

Annealing: hydroxyl groups on the Al_2O_3 surface

OH groups at the interface between copper and Al_2O_3 are known to be unstable well below annealing temperatures. Hydrogen gas in the furnace penetrates the thin film and reacts to form water vapor. Water vapor escaping through the annealing film would likely disrupt the Cu crystal lattice. The role this plays in the formation of a single crystal thin film is unknown.

Discussion about annealing

Thermal energy transferred into the thin film allows for annealing. The preferred direction and rate of the temperature gradient during annealing that leads to a single crystal thin film is unknown. The current study, like the Miller study, used a hot wall tube furnace. This setup eliminates the possibility that heat is transferred up through the substrate to the substrate/copper interface and on up through the thin film; as would be the case in of a heated-stage-type furnace. To reiterate, the thin film is being heated and annealed starting from the exterior surface.

Contrast that with the implications of Miller's work that the transition from OR II to OR I must be initiated at the interface between Al_2O_3 and Cu consequent to the change in strain at annealing temperature. The exact dynamics of the transition is unknown, but it seems likely that site hopping at the interface initiates a wave of recrystallization out through the thin film. This initiation site is most likely at the triple interface of the substrate, thin film and sample boundary. Since, the pre-annealed thin film is OR II, the entire thin film must undergo recrystallization in order to realize the OR I mono-crystalline final product.

Alternatively, Xu informs that a sweeping melt zone is consistently used to form a (111) single-crystal surface. Xu requires that the local temperature be above melting for recrystallization. It is conceivable that Miller is not too dissimilar from Xu with the difference that some of the energy for Miller's recrystallization comes from the stored energy in the pre-annealed disordered crystal. In this conception, both methods depend on the spontaneous formation of a properly oriented seed crystal to guide recrystallization across the sample.

In this way, the Miller process is the minimalist realization of the zone melting process. To recrystallize the surface to be a single crystal at the lowest temperature, requires that a perfectly prepared pre-annealed thin film is preloaded with a suitable energy profile in the form of crystal defects. It seems clear that if the stored energy profile is incorrect then recrystallization will fail.

A final thought is that the Miller method may be more readily replicated if samples were annealed in a sweeping manor like in the Xu method, starting from a corner of the sample. This may improve the odds of generating a single seed crystal that spread across the surface.

SUMMARY

The current study explored improvements to a graphene catalyst. A continuous smooth Cu thin film supported by polished Al_2O_3 was constructed, and this sample appears to have the qualities of a superior graphene substrate. Replication of the sample, however, was unsuccessful. Tighter control of processing parameters would likely improve the chances of reproducing such a delicate structure.

ACKNOWLEDGEMENTS

Vesa-Matti Hiltunen, Alexandra Elbakyan

APPENDIX I: CRYSTALLOGRAPHY

Crystal planes

A plane within a Bravais crystal lattice may be defined using the Miller index which is determined as follows: 1) Determine the intercepts of the plane with the axes measured in units of the lattice vectors. 2) Take the reciprocal of each number. 3) Scale the set of coordinates to the lowest value of integers with the same ratio; this is the Miller index for the plane, and it is written in the form (hkl). [Example: Step 1) $(-1,2,\infty)$. Step 2) $(-1, 1/2, 1/\infty)$. Step 3) $(\bar{2}\ 1\ 0)$]
A family of planes with equivalent lattice symmetry is written using curly brackets, $\{hkl\}$.

Crystal directions

Within the crystal lattice, directions use the square bracket notation in the form $[hkl]$, and the terms have units of the corresponding lattice vectors. A family of symmetrically equivalent directions uses the notation $\langle hkl \rangle$. The notation {*hkl*} denotes the set of all planes that have equivalent lattice symmetry to the plane (*hkl*). Figure 23 illustrates some directions within the FCC close packed plane (111), where

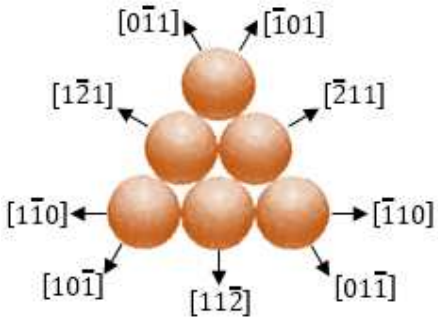

Figure 23 Directions in the (111) plane of a face centered cubic lattice. The <110> family are in the close packed direction.

For FCC and hexagonal lattices, when the Miller indices of a plane match those of a direction then the two are orthogonal.

Crystal defects: twinning

Twinning is a stacking defect of {111} planes. A twin occurs when the ABC stacking order of FCC (face centered cubic) layers mistakenly stacks in ABA order like HCP. The expected surface plane on the Cu thin film in this research is the (111) plane. When twinning occurs parallel to the surface, no surface damaging effect is expected. However, when twinned islands occur, the interface between the twinned and non-twinned regions form a crystal boundary. Atoms are not closed packed in the crystal boundary. As vertical growth continues, during thin-film deposition, the crystal boundary remains as a persistent defect on the film's surface. This is undesirable.

Twinning is initiated when a {111} boundary acquires new layers and the layer is added in the wrong manner. During copper growth in the [111] direction there is a low binding energy difference

between atoms that occupy the FCC locations and atoms that stack in faulted lattice sites, HCP locations. These lattice faults result in extensive nucleation of twin domains. Because the binding energy on the (111) plane of the surface is low, domains may rapidly expand or contract laterally. However, domain boundary motion in the direction of growth, that is, into the bulk of the crystal, requires much more energy, about 100 times more, so twin domain growth is restricted to the (111) plain. The resulting copper growth exhibits layer-by-layer twinning. And since the in-plane restructure rate is very fast, twinning is not affected much by deposition rate or temperature. Twin stacking is normal to the growth plane and few forces exist to coarsen the surface. [59]

Twinning does not occur when a {100} boundary migrates by consuming a {111} grain boundary.[58]

Crystal defects: voids

When domain boundary movement occurs on the surface, vacancies are filled by mobile surface atoms. However, when domain boundaries are contained within the bulk, vacancies are formed which require relatively high activation energy (0.7 eV) to diffuse.[59] Atoms arrive at the surface with velocities between 1000 and 1200 m/s.[60] Therefore the kinetic energy $\left(E_k = \frac{1}{2}mv^2\right)$ delivered by each copper atom is only between 0.33 and 0.47 eV, and insufficient to induce vacancy diffusion. So, a significant source of trapped vacancies is domain boundaries.

Crystal defects: Dislocations

Layer growth of a (111) plane proceeds as adatoms fill in space by close packing. Filling may proceed in the order of an FCC model where layers arrange ABCABC or in the order of an HCP where layers arrange ABAB (see Figure 24). Where the two grains meet voids are created. And when the next layer grows atop this grain boundary the atoms cannot stack in close packed formation but fall into positions which are dislocated from a uniform stacking order.

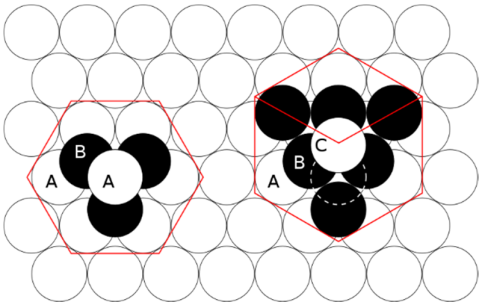

Figure 24 Hexagonal close packed (HCP) lattice (left) and face centered cubic (FCC) lattice (right). The red outline helps visualize the Bravais lattice. Letters indicate the translational position of layer, where hcp is stacked ABAB, and fcc is stacked ABCABC. The dashed circle indicates the location of a sphere in an A layer for comparison with the C position. (en.wikipedia.org/wiki/Close-packing_of_equal_spheres)

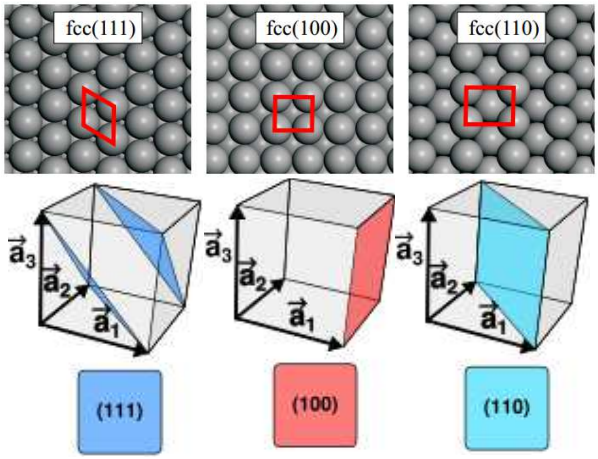

Figure 25 Structure of three crystal lattice planes in FCC crystals.

APPENDIX II: AL_2O_3

Physical Properties of α-Al_2O_3 [65]

Crystal Structure Hexagonal	a = 4.758 Å c = 12.992 Å
Crystallographic D spacing	(11$\underline{2}$0) - a plane: 2.379 Å (1$\underline{1}$02) - r plane: 1.740 Å (10$\underline{1}$0) - m plane: 1.375 Å (11$\underline{2}$3) - n plane: 1.147 Å (0001) - c plane: 2.165 Å (10$\underline{1}$1) - s plane: 1.961 Å
Melt Point	2040 °C
Density	3.98 g/cm^3
Hardness	9 (mohs)
Thermal Expansion	7.5 (x10^{-6} /°C)
Specific Heat	0.10 (cal /°C)
Thermal Conductivity	46.06 @ 0 °C 25.12 @ 100 °C 12.56 @ 400 °C (W/(m.K))
Dielectric Constant	~ 9.4 @ 300K at A axis ~ 11.58 @ 300K at C axis

Aluminum oxide (Al_2O_3) is commonly called alumina, and sometimes called aluminum oxide, corundum, or sapphire. The powdered form may be fused by heat to form crystalline arrangements of varying stability. The most stable being α-Al_2O_3 which is also called corundum and in its pure form is colorless and transparent. Intermixed with magnetite or hematite corundum becomes the mineral emery. If some of the Al^{3+} in corundum are substituted for other metals, gemstones can be formed. For example the following dopants make colored gems: Fe, Ti—blue sapphire; Cr—red ruby; Fe^{3+}, Fe^{2+}—yellow topaz; Fe, Mn, Ti—purple amethyst; Fe^{2+}—green emerald.

The alpha comes from an old naming convention for different compounds with the same composition. Chemical analysis reveals that heating aluminum hydroxide produces water vapor at temperatures below 1200 °C, and develops no steady weight. The compound becomes stable only after being heated above 1200 °C. So, the stable form of alumina was named the alpha form.[66]

α-Al_2O_3 structure can be derived by first arranging O^{2-} anions in a hexagonally close packed array with ABAB stacking. Second, place Al^{3+} cations in the octahedral holes such that 1/3 of the holes are left vacant. The vacancies are oriented in such a way that along the c-direction the Al^{3+} cations form a hexagonal lattice and the successive layers of anions have ABCABC stacking. Finally, the structure is allowed to relax as cations shift apart and press toward the vacancies. The resulting α-Al_2O_3 structure has a unit cell of 12 Al and 18 O, see Figure 27.

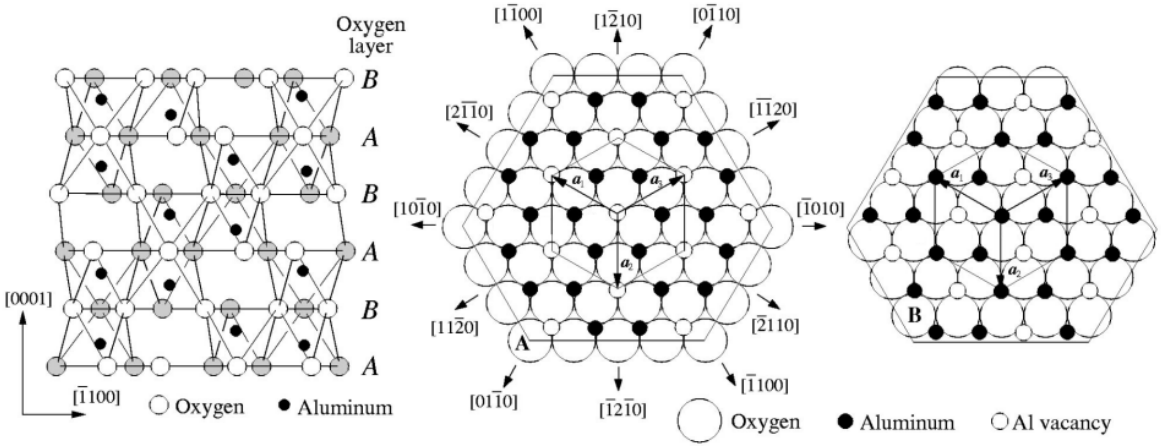

Figure 26 ***Bulk structure of α-Al_2O_3. Left:*** *A slice, one Al-octahedron thick (black lines indicate coordination), showing the stacking sequence (white-oxygen above, gray-oxygen below, black-Al between) in the [0001] direction.* ***Middle:*** *An "A" layer in the c-plane (0001) showing the family of $\langle 11\bar{2}0 \rangle$ translational vectors, O^{2-} (large white circles) below with Al^{3+} (small black circles) above. The octahedral hollows (small white circles) between two O^{2-} layers.* ***Right:*** *A "B" layer in the c-plane, rotated ~60° from the "A" layer. Large hexagon shows alignment of "A" and "B" layers. The hexagonal (trigonal) unit is cell is shown; with in-plane "a" axes and "c" axis out of the page (not shown).*[67,68]

The idealized crystal structure of Al_2O_3 is hexagonal close-packed (HCP) with a basis.

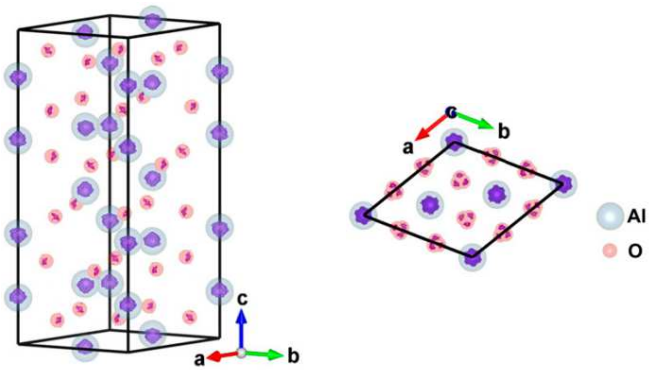

Figure 27 Experimentally determined α-Al_2O_3 unit cell with 12 Al and 18 O.[69,70]

The reported lattice constants of α-Al_2O_3 were measured using the proposed atomic-scale length standard, the wavelength of the Fe Mössbauer radiation. At room temperature, $T = 295.65$ K, the values are $a = 4.759213$ Å, $c = 12.991586$ Å.[71]

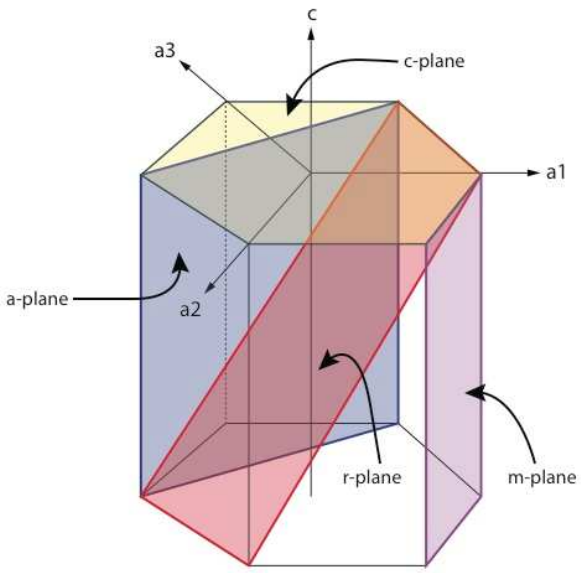

Figure 28 Single crystal sapphire planes commonly used include the a, c, m, and r-planes.[72] *The Miller index for the c-plane is (0001).*

APPENDIX III: COPPER

Technical data for Copper

Data provided by Mathematica's ElementData function from Wolfram Research, Inc.
[http://www.periodictable.com/Elements/029/data.html]

Overview	
Name	Copper
Symbol	Cu
Atomic Number	29
Atomic Weight	63.546
Thermal properties	
Melting Point	1084.62 °C
Boiling Point	2927 °C
Heat of Fusion	13.1 kJ/mol
Heat of Vaporization	300 kJ/mol
Specific Heat	384.4 J/(kg K)[solid phase]
Thermal Conductivity	400 W/(m K)
Thermal Expansion	$0.0000165\ K^{-1}$
Bulk physical properties	
Density (Solid)	$8.92\ g/cm^3$
Density (Liquid)	$8.02\ g/cm^3$
Molar Volume	7.124×10^{-6}
Mohs Hardness	3 MPa
Vickers Hardness	369 MPa
Bulk Modulus	140 GPa
Shear Modulus	48 GPa
Young Modulus	130 GPa
Poisson Ratio	0.34
Speed of Sound	3570 m/s
Thermal Conductivity	400 W/(m K)
Thermal Expansion	$0.0000165\ K^{-1}$
Classifications	
Block, Group, Period	d, 11, 4
Electron Configuration	$[Ar]3d^{10}4s^1$
Electrical properties	
Electrical Conductivity	5.9×10^7 S/m
Resistivity	1.7×10^{-8} m Ω
Magnetic properties	
Magnetic Type	Diamagnetic
Mass Magnetic Susceptibility	-1.08×10^{-9}
Molar Magnetic Susceptibility	-6.86×10^{-11}
Volume Magnetic Susceptibility	-9.63×10^{-6}
Atomic dimensions and structure	
Atomic Radius	145 pm
Covalent Radius	138 pm
Van der Waals Radius	140 pm
Crystal Structure	Face Centered Cubic
Lattice Angles	π/2, π/2, π/2
Lattice Constants	361.49, 361.49, 361.49 pm

Face centered cubic (FCC)

The crystal structure of copper is face centered cubic (FCC). The FCC unit cell contains the equivalent of 4 atoms; $8 \times \frac{1}{8} + 6 \times \frac{1}{2}$ (see Figure 29). An *x,y,z* coordinate system may be assigned with the origin at a vertex of the unit cell and orthogonal axes along the corresponding edges. Three lattice vectors, *a,b,c,* are assigned in the directions of the *x,y,z* axis with lengths equal to the length of the unit cell (lattice constants) in the corresponding directions.

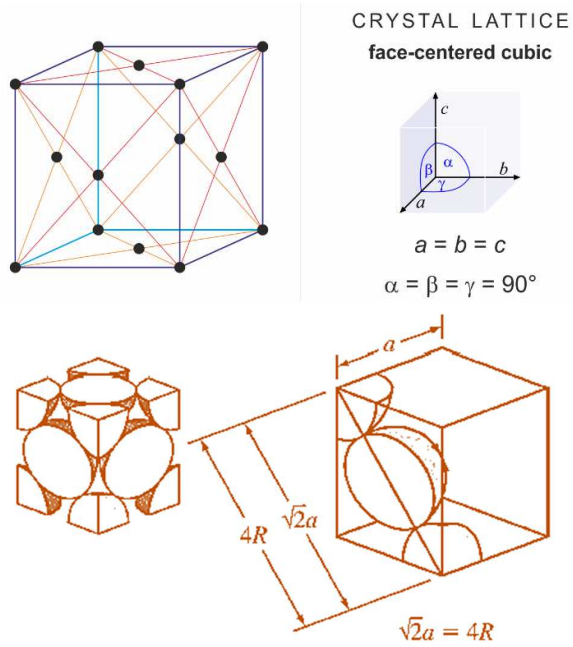

Figure 29 Face centered cubic. ***Top****: orthogonal axes and lattice vectors of equal length.*
Bottom*: Lattice constant (a) as a function of atomic radius (R).*

Crystallographic defects in Cu

The subject of this research is the manufacture of an as-smooth-as-possible Cu thin film; therefore, the following discussion about Cu defects limits itself to the defects within pure Cu. Neither the inclusion of non-Cu atoms within the thin-film nor the non-metal bonds (covalent bonds) at the substrate interface are addressed here. The former is expected to be minimized by the near vacuum environment during deposition of the thin-film. The latter is expected to have no significant effect on the surface of the film of interest here.

Stacking faults

Any arrangement of Cu atoms that deviates from a perfect FCC crystal structure is a stacking fault. The two simplest faults are 1) a vacancy, in which an atom is missing from a site in the regular lattice structure, and 2) an interstitial, in which an atom is positioned at a site displaced from the regular lattice sites. All crystal stacking faults can be conserved as combinations of these two simple stacking faults.

A common crystal fault in copper is slip along the close packed plane Cu(111) where the FCC stacking is replaced by HCP stacking. That is, ABC stacking of planes is replaced by ABA stacking of planes; in this way a crystal twin is generated.

As deposited, the thin film contains many complicated arrangements of crystals and stacking faults. Predictive fault models are unavailable, so optimization is accomplished by experimentation. And while x-ray diffraction (XRD) and electron backscatter diffraction (EBSD) are techniques can measure crystalline micro-structure, these were not available for use in this study.

CITATIONS

1. Geim, A. K. & Novoselov, K. S. The rise of graphene. *Nat. Mater.* **6,** 183–191 (2007).

2. Orofeo, C. M. *et al.* Influence of Cu metal on the domain structure and carrier mobility in single-layer graphene. *Carbon N. Y.* **50,** 2189–2196 (2012).

3. Luo, Z. *et al.* Effect of substrate roughness and feedstock concentration on growth of wafer-scale graphene at atmospheric pressure. *Chem. Mater.* **23,** 1441–1447 (2011).

4. Yan, Z., Peng, Z. & Tour, J. M. Chemical vapor deposition of graphene single crystals. *Acc. Chem. Res.* **47,** 1327–37 (2014).

5. Li, X. *et al.* Large-area synthesis of high-quality and uniform graphene films on copper foils. *Science* **324,** 1312–1314 (2009).

6. Bae, S. *et al.* Roll-to-roll production of 30-inch graphene films for transparent electrodes. *Nat. Nanotechnol.* **5,** 574–578 (2010).

7. Wang, L. G., Šob, M. & Zhang, Z. Instability of higher-energy phases in simple and transition metals. *J. Phys. Chem. Solids* **64,** 863–872 (2003).

8. Blaha, P., Schwarz, K., Sorantin, P. & Trickey, S. B. Full-potential, linearized augmented plane wave programs for crystalline systems. *Comput. Phys. Commun.* **59,** 399–415 (1990).

9. Li, R. *et al.* Stacking fault energy of face-centered cubic metals: Thermodynamic and ab initio approaches. *J. Phys. Condens. Matter* **28,** (2016).

10. Grabowski, B., Söderlind, P., Hickel, T. & Neugebauer, J. Temperature-driven phase transitions from first principles including all relevant excitations: The fcc-to-bcc transition in Ca. *Phys. Rev. B - Condens. Matter Mater. Phys.* **84,** (2011).

11. Patala, S., Mason, J. K. & Schuh, C. A. Improved representations of misorientation information for grain boundary science and engineering. *Prog. Mater. Sci.* **57,** 1383–1425 (2012).

12. Jaynes, E. T. The Well-Posed Problem. *Found. Phys.* **3,** 477–492 (1973).

13. Tobergte, D. R. & Curtis, S. The Solubility of Carbon in Solid Gold, Copper, and Silver. *Scr. Metall.* **3,** 389–392 (1969).

14. López, G. A. & Mittemeijer, E. J. The solubility of C in solid Cu. *Scr. Mater.* **51,** 1–5 (2004).

15. Muñoz, R. & Gómez-Aleixandre, C. Review of CVD synthesis of graphene. *Chem. Vap. Depos.* **19,** 297–322 (2013).

16. Hofrichter, J. *et al.* Synthesis of graphene on silicon dioxide by a solid carbon source. *Nano Lett.* **10,** 36–42 (2010).

17. Hu, B. *et al.* Epitaxial growth of large-area single-layer graphene over Cu(111)/sapphire by atmospheric pressure CVD. *Carbon N. Y.* **50,** 57–65 (2012).

18. Chambers, S. A., Droubay, T., Jennison, D. R. & Mattsson, T. R. Laminar growth of ultrathin metal films on metal oxides: Co on hydroxylated α-Al2O3(0001). *Science (80-.).* **297,** 827–831 (2002).

19. Katz, G. The Epitaxy of Copper on Sapphire. *Appl. Phys. Lett.* **12,** 161 (1968).

20. Gottstein, G. & Shvindlerman, L. S. *Grain Boundary Migration in Metals: Thermodynamics, Kinetics, Applications*. (Taylor & Francis, 1999).

21. Miller, D. L., Keller, M. W., Shaw, J. M., Chiaramonti, a N. & Keller, R. R. Epitaxial (111) films of Cu, Ni, and CuxNiy on alpha-Al2O3 (0001) for graphene growth by chemical vapor deposition. *J. Appl. Phys.* **112,** 1–9 (2012).

22. Bialas, H. & Knoll, E. Heteroepitaxy of copper on sapphire under uhv conditions. *Vacuum* **45,** 959–966 (1994).

23. Thompson, C. V., Floro, J. & Smith, H. I. Epitaxial grain growth in thin metal films. *J. Appl. Phys.* **67,** 4099–4104 (1990).

24. Mishin, Y. An Atomistic View of Grain Boundary Diffusion. *Defect Diffus. Forum* **363,** 1–11 (2015).

25. Klokholm, E. & Berry, B. S. Intrinsic Stress in Evaporated Metal Films. *J. Electrochem. Soc.* **115,** 823- (1968).

26. Niu, C. *et al.* Cu interactions with α-Al2O3(0001): Effects of surface hydroxyl groups versus dehydroxylation by Ar-ion sputtering. *Surf. Sci.* **465,** 163–176 (2000).

27. Scheu, C. *et al.* Bonding at copper-alumina interfaces established by different surface treatments: A critical review. *J. Mater. Sci.* **41,** 5161–5168 (2006).

28. Eng, P. J. *et al.* Structure of the Hydrated α-Al2O3 (0001) Surface. *Science (80-.).* **288,** 1029–1033 (2000).

29. Oh, S., Scheu, C., Wagner, T., Tchernychova, E. & Ruhle, M. Epitaxy and bonding of Cu films on oxygen-terminated α-Al2O3(0001) surfaces. *Acta Mater.* **54,** 2685–2696 (2006).

30. Curiotto, S. *et al.* Orientation relationships of copper crystals on c-plane sapphire. *Acta Mater.* **59,** 5320–5331 (2011).

31. Tsyganenko, A. A. & Mardilovich, P. P. Structure of alumina surfaces. *J. Chem. Soc. Faraday Trans.* **92,** 4843 (1996).

32. Knözinger, H. & Ratnasamy, P. Catalytic Aluminas : Surface Models and Characterization of Surface Sites. *Catal. Rev.* **17,** 31–70 (1978).

33. Reddy, K. M., Gledhill, A. D., Chen, C.-H., Drexler, J. M. & Padture, N. P. High quality, transferrable graphene grown on single crystal Cu(111) thin films on basal-plane sapphire. *Appl. Phys. Lett.* **98,** 113117 (2011).

34. Guo, Q. & Møller, P. J. On the thermal stability of copper deposits on a (0001) sapphire surface. *Surf. Sci.* **244,** 228–236 (1991).

35. Gautier, M., Pham Van, L. & Duraud, J. ~P. Copper Clusters Formation on Al2O3 Surfaces: an XPS and SEXAFS study. *Eur. Lett.* **18,** 175–180 (1992).

36. Dehm, G., Scheu, C., Mobus, G., Brydson, R. & Ruhle, M. Synthesis of analytical and high-resolution transmission electron microscopy to determine the interface structure of Cu / Al2O3. *Ultramicroscopy* **67,** 207–217 (1997).

37. Kelber, A., Niu, C., Shepherd, K. & Jennison, D. R. Copper Wetting of α-Al2O3(0001): Theory and Experiment. *Surf. Sci.* **446,** 76–88 (2000).

38. Burgess, J. F. The Direct Bonding of Metals to Ceramics by the Gas-Metal Eutectic Method. *J. Electrochem. Soc.* **122,** 688 (1975).

39. Seager, C. W., Kokini, K., Trumble, K. & Krane, M. J. M. The influence of CuAlO2 on the strength of eutectically bonded Cu/Al2O3 interfaces. *Scr. Mater.* **46,** 395–400 (2002).

40. Zhang, W., Smith, J. R. & Evans, A. G. The connection between ab initio calculations and interface adhesion measurements on metal/oxide systems: Ni/Al2O3 and Cu/Al2O3. *Acta Mater.* **50,** 3803–3816 (2002).

41. Oh, S. H., Scheu, C., Wagner, T. & Rühle, M. Control of bonding and epitaxy at copper/sapphire interface. *Appl. Phys. Lett.* **91,** (2007).

42. Sasaki, T. *et al.* Atomic and electronic structures of Cu/alpha-Al2O3 interfaces prepared by pulsed-laser deposition. *Sci. Technol. Adv. Mater.* **4,** 575–584 (2003).

43. Miller, D. L. *et al.* Giant secondary grain growth in Cu films on sapphire. *AIP Adv.* **3,** 1–10 (2013).

44. Ogawa, Y. *et al.* Domain structure and boundary in single-layer graphene grown on Cu(111) and Cu(100) films. *J. Phys. Chem. Lett.* **3,** 219–226 (2012).

45. Konishi, S., Moriyama, M. & Murakami, M. Effect of Annealing Atmosphere on Void Formation in Copper Interconnects. *Mater. Trans.* **43,** 1624–1628 (2002).

46. Brongersma, S. H. Grain Structure Evolution During Annealing of Electroplated Copper. *AIP Conf. Proc.* **612,** 229–234 (2002).

47. Choubak, S., Biron, M., Levesque, P. L., Martel, R. & Desjardins, P. No Graphene Etching in Purified Hydrogen. *J. Phys. Chem. Lett.* **4,** 1100–1103 (2013).

48. Lewis, A. M., Derby, B. & Kinloch, I. A. The Influence of Gas Phase Equilibria on the Chemical Vapor Deposition of Graphene. *ACS Nano* **7,** 3104–3117 (2013).

49. Bhaviripudi, S., Jia, X., Dresselhaus, M. S. & Kong, J. Role of kinetic factors in chemical vapor deposition synthesis of uniform large area graphene using copper catalyst. *Nano Lett.* **10,** 4128–33 (2010).

50. Pang, J. *et al.* Oxidation as A Means to Remove Surface Contaminants on Cu Foil Prior to Graphene Growth by Chemical Vapor Deposition. *J. Phys. Chem. C* **119,** 13363–13368 (2015).

51. Asif, M. *et al.* Thickness controlled water vapors assisted growth of multilayer graphene by ambient pressure chemical vapor deposition. *J. Phys. Chem. C* **119,** 3079–3089 (2015).

52. Goli, P. *et al.* Thermal Properties of Graphene - Copper - Graphene Heterogeneous Films. *Nano Lett.* 1–5 (2014). doi:10.1021/nl404719n

53. Goli, P. *et al.* Strong Enhancement of Thermal Properties of Copper Films after Chemical Vapor Deposition of Graphene. 1–16 (2013).

54. Hao, Y. *et al.* The role of surface oxygen in the growth of large single-crystal graphene on copper. *Science* **342,** 720–3 (2013).

55. Miller, D. L. *et al.* Supplementary Information for Giant Secondary Grain Growth in Cu Films on Sapphire. 1–6 (2013).

56. Xu, X. *et al.* Ultrafast epitaxial growth of metre-sized single-crystal graphene on industrial Cu foil. *Sci. Bull.* **62,** 1074–1080 (2017).

57. Xu, X. *et al.* Ultrafast growth of single-crystal graphene assisted by a continuous oxygen supply. *Nat. Nanotechnol.* **11,** 930–935 (2016).

58. Patten, J. W., McClanahan, E. D. & Johnston, J. W. Room-temperature recrystallization in thick bias-sputtered copper deposits. *J. Appl. Phys.* **42,** 4371–4377 (1971).

59. Zhou, X. W. & Wadley, H. N. G. Twin formation during the atomic deposition of copper. *Acta Mater.* **47,** 1063–1078 (1999).

60. ASANO, T., UETAKE, N. & SUZUKI, K. Mean Atomic Velocities of Uranium, Titanium and Copper during Electron Beam Evaporation. *J. Nucl. Sci. Technol.* **29,** 1194–1200 (1992).

61. DeHaven, P. W. *et al.* US6638374B2.pdf. 8 (2003).

62. Gangulee, A. The Structure of Electroplated and Vapor-Deposited Copper Films. *J. Appl. Phys.* **43,** 867–873 (1972).

63. Gangulee, A. The Structure of Electroplated and Vapor-Deposited Copper Films. II. Effects of Annealing. *J. Appl. Phys.* **43,** 3943–3948 (1972).

64. Gangulee, A. The Structure of Electroplated and Vapor-Deposited Copper Films. III. Recrystalization and Grain Growth. *J. Appl. Phys.* **45,** 3749–3756 (1974).

65. MTI-Corporation. Al 2 O 3 Single Crystal Sapphire boule and polished wafer. *http://www.mtixtl.com/*

66. Santos, P. S., Santos, H. S. & Toledo, S. P. Standard transition aluminas. Electron microscopy studies. *Mater. Res.* **3,** 104–114 (2000).

67. Ruberto, C., Yourdshahyan, Y. & Lundqvist, B. I. Surface properties of metastable alumina: A comparative study of κ- and α−Al2O3. *Phys. Rev. B* **67,** 195412 (2003).

68. Dobrovinskaya, E. R., Lytvynov, L. A. & Pishchik, V. *Sapphire: Material, Manufacturing, Applications*. (Springer Science + Business Media, LLC, 2009). doi:10.1007/978-0-387-85695-7

69. Nakashima, P. N. H., Moodie, A. F. & Etheridge, J. Direct atomic structure determination by the inspection of structural phase. *Proc. Natl. Acad. Sci. U. S. A.* **110,** 14144–9 (2013).

70. Lewis, J., Schwarzenbach, D. & Flack, H. D. Electric field gradients and charge density in corundum, α-Al 2 O 3. *Acta Crystallogr. Sect. A* **38,** 733–739 (1982).

71. Shvyd'ko, Y. V. *et al.* Measuring wavelengths and lattice constants with the Mössbauer wavelength standard. *J. Synchrotron Radiat.* **9,** 17–23 (2002).

72. Shape. Available at: http://blog.clearlysapphire.com/wp-content/uploads/2014/12/Shape.jpg.

73. Chen, X., Zhang, L. & Chen, S. Large area CVD growth of graphene. *Synth. Met.* **210,** 95–108 (2015).

74. Knorr, D. B. & Tracy, D. P. A review of microstructure in vapor deposited copper thin films. *Mater. Chem. Phys.* **41,** 206–216 (1995).